FLEXURAL STRENGHENING OF RC CONTINUOUS SLAB STRIPS USING NSM CFRP LAMINATES

Gláucia M. Dalfré [1], Joaquim A.O Barros [1,2]

[1] ISISE, University of Minho, Guimarães, Portugal; [2] Corresponding Author

ABSTRACT

To assess the effectiveness of the near surface mounted (NSM) technique, in terms of load carrying and moment redistribution capacities, for the flexural strengthening of continuous reinforced concrete (RC) slabs, an experimental program was carried out. The experimental program is composed of three series of three slab strips of two equal span length, in order to verify the possibility of increasing the negative (at the intermediate support region) resisting bending moment in 25% and 50% and maintaining moment redistribution levels of 15%, 30% and 45%. Though the flexural resistance of the NSM strengthened sections has exceeded the target values, the moment redistribution was relatively low, and the increase of the load carrying capacity of the strengthened slabs did not exceed 25%. This experimental program is analyzed to highlight the possibilities of NSM technique for statically indeterminate RC slabs in terms of flexural strengthening effectiveness, moment redistribution and ductility performance. Using a FEM-based computer program, which predictive performance was appraised using the obtained experimental results, a high effective NSM flexural strengthening strategy is proposed, capable of enhancing the slab's load carrying capacity and maintaining high levels of ductility.

KEYWORDS: Continuous RC slabs, Flexural strengthening, CFRP, NSM, Moment redistribution

1. INTRODUCTION

Gluing fibre reinforced polymer (FRP) laminates by a structural adhesive into thin slits cut on the concrete cover of reinforced concrete (RC) elements is a strengthening technique, designated Near Surface Mounted (NSM), which is gaining increasing attention of practitioners, engineers and scientists interested in structural rehabilitation. The efficacy of the NSM technique for the flexural strengthening of RC structures has been proven by research and applications (Nanni *et al.* 2004). This efficacy has been explored, mainly to increase the positive bending moments of statically determinate RC beams (Blaschko and Zilch 1999; El-Hacha and Rizkalla 2004; Barros and Fortes 2005,

Kotynia 2006) and slabs (Barros *et al.* 2008; Bonaldo *et al.* 2008). However, due to the characteristics of the application of this strengthening technique, it is particularly appropriate to increase the negative bending moments (developed at the interior supports) of continuous (two or more spans) RC slabs. In fact, the opening process of the slits can be easily executed by the equipment used to open crack control joints in concrete slabs.

When a continuous RC structure is strengthened with FRP materials, its ductility and plastic rotation capacity may be, however, restricted or even extinct, due to, principally, the linear-elastic tensile behaviour of the FRP up to its brittle failure (Arduini *et al.* 1997, Casadei *et al.* 2003). As flexural members retrofitted with externally bonded reinforcing (EBR) technique tend to fail by brittle premature plate debonding well before the FRP tensile strength capacity is reached, the ductility, particularly the plastic rotation capacity, can be severely reduced, decreasing the available degree of moment redistribution (Oehlers *et al.* 2004a). The tests of El-Refaie *et al.* (2003a, 2003b), Ashour *et al.* 2004 and Oehlers *et al.* (2004a) show that, in general, premature debonding of the external strengthening system is the dominant failure mechanism. However, according to the approach used by these authors to quantify the moment redistribution, significant moment redistribution was obtained in the tests (El-Refaie *et al.* 2003a, Oehlers *et al.* 2004a/2004b, Oehlers *et al.* 2006, Liu *et al.* 2006a), which contradicts the existing design guidelines (Concrete Society 2000, fib 2001, ACI 440 2007) that suggest that moment redistribution should not be allowed for RC members strengthened with EBR technique.

On the other hand, tests with simply supported RC members strengthened with NSM strips (Hassan and Rizkalla 2003, Täljsten *et al.* 2003, Barros *et al.* 2007) have shown that NSM strengthening elements debond or fail at much higher strain than EBR strengthening systems, therefore, in general, NSM strengthened members are expected to have a much more ductile behaviour than EBR strengthened members. Therefore, NSM technique seems to have high potential for the strengthening of negative bending moment regions, since relatively easy and fast strengthening procedures are required.

The first preliminary studies on moment redistribution of statically indeterminate RC members strengthened with NSM technique were conducted at the Adelaide University, in Australia (Liu *et al.* 2006b). A significant amount of moment redistribution was attained using NSM technique, when compared with EBR technique. Park and Oehlers (2000) performed tests on a series of continuous beams strengthened with externally bonded steel or FRP reinforcement over the positive (sagging) and negative (hogging) bending moments regions. The plates were applied on either the tension face or the side faces of the beam. For both steel and FRP plated beams, plate debonding was observed. This indicates that, although steel is a ductile material, the externally bonded steel plates can still reduce the ductility of the retrofitted beam, depending on the plating dimensions and positions, and almost zero moment redistribution was obtained in all the tests. Ashour *et al.* (2004) performed tests on sixteen RC continuous beams

with different arrangements of internal and external reinforcement. All beams were strengthened with CFRP sheets or plates over the hogging and/or sagging regions. All strengthened beams exhibited a higher load capacity but lower ductility compared with their respective unstrengthened control beams.

Recently, Bonaldo (2008) carried out an experimental program to assess the moment redistribution capacity of two-way RC slabs flexural strengthened with NSM CFRP laminates. In spite of the increase of the flexural resistance of the sections at the hogging region has exceeded the target values (25% and 50%), the moment redistribution was relatively low, and the increase of the load carrying capacity of the strengthened slabs was limited to 21%. In the present work, this experimental program is analyzed in depth in order to assess the possibilities and challenges of the NSM technique in terms of flexural strengthening effectiveness, moment redistribution and ductility performance of continuous RC slabs. Using the results obtained in the experimental program, the predictive performance of a constitutive model implemented into a FEM-based computer program was appraised. With the help of this computer program, a high effective NSM flexural strengthening strategy is proposed, capable of enhancing the slab's load carrying capacity and assuring high levels of ductility (Bonaldo *et al.* 2008).

2. THE EXPERIMENTAL PROGRAM

2.1 Slab specimens and strengthening technique

According to CEB-FIB Model Code (1993), the coefficient of moment redistribution, $\delta = M_{red}/M_{elas}$, is defined as the relationship between the moment in the critical section after redistribution (M_{red}) and the elastic moment (M_{elas}) in the same section calculated according to the theory of elasticity, while $\eta = (1 - \delta) \times 100$ is the moment redistribution percentage. To assess the influence of NSM flexural strengthening technique, using CFRP laminates, on the moment redistribution capability of continuous RC slabs, an experimental program composed of nine 120×375×5875 mm^3 RC two-way slabs was carried out (Figure 1a). Three of the RC slabs were unstrengthened, forming a control set (SL15, SL30 and SL45), and six slabs were strengthened with CFRP laminates according to the NSM technique (SL15s25, SL15s50, SL30s25, SL30s50, SL45s25 and SL45s50, Figure 1a to 1e). The notation adopted to identify each slab specimen is SLxsy, where SL is the slab strip base, x is the moment redistribution percentage, η, (15%, 30% or 45%), s means that the slab is strengthened, and y is the increase of the negative resisting bending moment of the slab cross section at the hogging region (25% or 50%). The concrete cover thickness for both the top and bottom reinforcements is about 26 mm. Figure 1 and Table 1 show the geometry and the reinforcement and strengthening details of the cross sections of the slabs of the experimental program. These reinforcement arrangements were designed for a load of F=50.82 kN, which is 10% higher the load for the verification of deflection service limit state according to ACI 318 (2004). The steel reinforcement was designed

according to the Eurocode 2 (2004) recommendations, while the NSM CFRP strips were designed following the suggestions of ACI 440 (2007), taking for effective strain, ε_{fd}, 70% the ultimate strain obtained in uniaxial tensile tests, ε_{fu}. The design details of these slabs can be found elsewhere (Bonaldo 2008).

2.2 Test configuration and monitoring system

The loading and support conditions are represented in Figure 1a, while the disposition of the displacement transducers for measuring the slab's deflection is shown in Figure 2a. The LVDTs 60541 and 18897, positioned at the slab mid-spans, were also used to control the tests at a displacement rate of 20 μm/s up to the deflection of 50 mm. After this deflection, the actuators internal LVDTs were used to control the test at 25 μm/s displacement rate. The positioning of the strain gauges (SG) installed in steel bars, CFRP strips and concrete for the slabs of the SL15 series is represented in Figures 2b to 2f. For the other series, consult Bonaldo (2008). Ten electrical resistance strain gauges were installed on the internal steel reinforcement at the central support (SG1 to SG7, Figure 2b) and under line loads (SG8 to SG10, Figure 2c) to measure the strains in the steel reinforcements at relevant regions. Six strain gages (SG11 to SG16, Figure 2d) were bonded on concrete surface to assess the concrete compressive strain variation. Finally, three strain gages were installed at one CFRP laminate (SG17 to SG19, Figure 2e and 2f) to evaluate the strain variation along the laminate.

2.3 Materials properties

The values of the properties evaluated for the concrete, steel bars and CFRP laminates are included in Tables 2, 3 and 4, respectively. Details of how these properties were characterized can be found elsewhere (Bonaldo 2008).

2.4 Relevant results

The relationship between the load applied (F) in each loaded section of the two spans of the slab (see Figure 2a) and the corresponding deflection, for the three series, is represented in Figures 3. The target increase of negative resisting bending moment (ΔM^{-}_{Tar}), and the increase of negative bending moment (ΔM^{-}_{Exp}) determined from the force ($\overline{F}_{\max}$) and reaction ($\overline{R}_{L,\overline{F}_{\max}}$, $\overline{R}_{C,\overline{F}_{\max}}$) values registered experimentally are included in Table 5, being $\overline{F}_{\max}$ the maximum value of the average of the forces applied in the two spans, and $\overline{R}_{L,\overline{F}_{\max}}$ and $\overline{R}_{C,\overline{F}_{\max}}$ are the reactions at lateral and at central supports, respectively, at $\overline{F}_{\max}$. It is verified that, though the target increase in the negative resisting bending moment has been exceeded in the strengthened slabs (values in round brackets in the last column

of Table 5), an average increase of 8% and 16% was obtained for the load carrying capacity of the slabs strengthened for an increase of the negative bending moment of 25% and 50%, respectively (values in round brackets in the third column of Table 5). This can be justified by the analysis of the graphics of Figures 4 to 6 and values of Table 6. In this table, for each slab, the following data is supplied: the moment at loaded section (M^{+}_{static}) and at intermediate support (M^{-}_{static}) obtained by static equilibrium, the corresponding variation of negative bending moment (ΔM^{-}) and applied load (ΔF), the total load (F=50.82 kN+ΔF), the positive (M^{+}_{Rd}, at Section S_1-S_1', see Figure 1a) and negative (M^{-}_{Rd}, at Section S_2-S_2', see Figure 1a) resisting-bending moments, the last one calculated according to the recommendations of ACI 440 (detailed design can be found in Dalfré and Barros 2009a). In series SL15, to assure an increase of 25% and 50% of the negative resisting bending moment, the applied load should increases 12.71 kN and 25.41 kN, respectively, leading to a final values of positive bending moment of 30.29 and 36.35 kN.m (see also Figure 4). However, according to the reinforcement arrangement of section S_1-S_1' (Figures 1b to 1d), the resisting bending moment is 25.16 kN.m, which means that, the contribution of the laminates for the load carrying capacity of the slab is

$$\left[\frac{50.82[kN]+\Delta F[kN]}{2}+\frac{22.68[kN.m]+7.73[kN.m]}{2.8[m]}\right]\times 1.4[m]=25.16[kN.m]\Rightarrow \Delta F=6.84\ kN \quad (1)$$

which corresponds to an increase of 13%, similar to the value obtained experimentally. Performing similar analysis for the SL15s50 slab,

$$\left[\frac{50.82[kN]+\Delta F[kN]}{2}+\frac{22.68[kN.m]+16.02[kN.m]}{2.8[m]}\right]\times 1.4[m]=25.16[kN.m]\Rightarrow \Delta F=12.76\ kN \quad (2)$$

which corresponds to an increase of 25%, similar to the value obtained experimentally (21%). In case of SL30s25 and SL30s50 slabs the CFRP laminates can provide an increase of 10% and 19% in the load carrying capacity of these slabs that are similar to the obtained values (10% and 16%, respectively). Finally, for SL45s25 and SL45s50 slabs increase values of 10% and 17% in the load carrying capacity of these slabs are determined, which are similar to the obtained values (4% and 10%).

Therefore, to increase significantly the load carrying capacity of this type of slabs, the positive resisting bending moments need also to be increased, using, for instance, NSM CFRP laminates in the bottom tensile surface of the two spans of the slab.

Table 7 resumes the results obtained experimentally for two scenarios: when a plastic hinge formed at the hogging region (at intermediate support zone, IS); when a plastic hinge formed at the sagging region (at loaded section, LS).

In this Table, $\bar{F}_y^{IS}$ and $\bar{F}_y^{LS}$ are the average loads at the formation of the plastic hinge at IS and LS, respectively, $\bar{u}_y^{IS}$ and $\bar{u}_y^{LS}$ are the average deflection for $\bar{F}_y^{IS}$ and $\bar{F}_y^{LS}$, respectively, $\varepsilon_{c,max}^{IS}$ and $\varepsilon_{c,max}^{LS}$ are the maximum concrete strains at IS and LS, $\varepsilon_{s,max}^{IS}$ and $\varepsilon_{s,max}^{LS}$ are the maximum strains in steel bars at IS and LS, respectively, $\varepsilon_{f,max}$ is the maximum strain in the CFRP laminates, $\bar{F}$ is the average load when a concrete compressive strain of 3.5‰ was recorded at the IS ($\varepsilon_c^{IS} = -3.5‰$), and $\varepsilon_{f,max}^{\bar{F}}$ and $\varepsilon_{s,max}^{\bar{F}}$ are the maximum strains in the CFRP laminates and in steel bars at $\bar{F}$. It was assumed that a plastic hinge has formed when yield strain was attained at the steel bars of this region. The following remarks can be pointed out:

(i) After concrete crack initiation, the slab stiffness decreased significantly, but the elasto-cracked stiffness was almost maintained up to the formation of the plastic hinge at the hogging region;

(ii) Up to the formation of the plastic hinge at the hogging region the tensile strains in the laminates are far below their ultimate tensile strain. At concrete crushing (assumed as -3.5‰) the maximum tensile strain in the laminates did not exceed 60% of their ultimate tensile strain;

(iii) The force-deflection relationship evidences that, up to the formation of the plastic hinge at the hogging region, the laminates had a marginal contribute for the slabs load carrying capacity. The deflection at $\bar{F}_y^{LS}$, $\bar{u}_y^{IS}$, was not significantly affected by the presence of the laminates. At the formation of the plastic hinge in the hogging region, the maximum strains in the steel bars at the loaded sections, $\varepsilon_{s,max}^{LS}$, are as nearest the yield strain as smaller is the level of moment redistribution. Therefore, the increment of load between the formation of the plastic hinge at hogging and at sagging regions decreased with the decrease of moment redistribution and, for each series, in general, this increment decreased with the increase of the percentage of laminates;

(iv) As expected, $\bar{F}_y^{LS}$ was almost equal for all series because the M_{Rd}^{+} of all the slabs is similar (7th column of Table 6);

(v) At $\bar{F}_y^{LS}$, the $\varepsilon_{c,max}^{IS}$ and $\varepsilon_{c,max}^{LS}$ were as higher as larger was the moment redistribution. For the SL30 and SL45 series the $\varepsilon_{c,max}^{IS}$ exceeded the strain at uniaxial concrete compressive strength (ε_{c1}, see Table 8), *i.e.,* the concrete is in its compressive softening phase, while $\varepsilon_{c,max}^{LS}$ was almost attaining ε_{c1}. This also collaborates for the small contribution of the laminates for the slab load carrying capacity.

Figure 7 depicts the relationship between the average applied load and the moment redistribution percentage for the three tested slabs. It is visible that, in general, after the cracking load ($\bar{F}_{cr}$) the moment redistribution decreases up to the formation of the plastic hinge in the hogging region ($\bar{F}_y^{IS}$), followed by an increase of η up to the formation of the plastic hinge in the sagging regions ($\bar{F}_y^{LS}$). The decrease of η is due to the decrease of stiffness in the sagging regions

due to the crack formation and propagation in these zones. When the plastic hinge formed at the hogging region, the consequent loss of stiffness forced a migration of moments from the hogging to the sagging regions resulting an increase of η. The graphs of Figure 7 also show that η decreases with the increase of the percentage of CFRP laminates. At the formation of the plastic hinge in the sagging region the following η values are obtained: 18.8%, 4.6%, -1.8% for SL15, SL15s25, SL15s50; 38.4%, 26.0%, 18.7% for SL30, SL30s25, SL30s50, 52.9%, 42.9%, 35.7% for SL45, SL45s25, SL45s50. For a compressive strain of 3.5 ‰ in the concrete surface at loaded sections, the following values of η are obtained: 17.5%, -3.9%, -14.8% for SL15, SL15s25, SL15s50; 36.4%, 25.3%, 14.9% for SL30, SL30s25, SL30s50, 53.0%, 42.8%, 30.8% for SL45, SL45s25, SL45s50.

3. PREDICTING THE BEHAVIOUR OF CONTINUOUS NSM FLEXURAL STRENGTHENED RC SLABS

3.1 Introduction

For the prediction of the behaviour of RC continuous slabs strengthened with NSM laminate arrangements capable of increasing the load carrying capacity and assuring high level of ductility for this type of structure, a computer program, based on the finite element method (FEM), is used. This program includes constitutive models able of simulating the concrete crack initiation and crack propagation, the nonlinear concrete compression behaviour, the elasto-plastic behaviour of steel reinforcements and the elastic-brittle failure behaviour of FRP elements. According to the model selected, a concrete slab is considered as a plane shell formulated under the Reissner-Mindlin theory (Barros and Figueiras 2001). In order to simulate the progressive damage induced by concrete cracking and concrete compression nonlinear behaviour, the shell element is discretized in layers. Each layer is considered in a state of plane stress. A detailed description of this model can be found elsewhere (Barros *et al.* 2008).

3.2 Predictive performance of the model

The predictive performance of this model is assessed by simulating the tested slabs. Due to the structural symmetry, only half of the slab is considered in the numerical simulations. Figure 8 shows the eight node finite element mesh adopted to discretize the half part of the slab. The support conditions are also represented in this figure. The slab thickness is discretized in 20 layers. The values of the parameters of the constitutive models are indicated in Tables 8 to 10 (see also Figures 9 and 10 for the comprehension of the physical meaning of some parameters). To take into account that at the cracked section the stress in the steel reinforcement is higher than the stress between cracks, and considering that the model evaluates the average strains in the steel, the stress reduction factors for the σ_{sy}, σ_{sh}, and σ_{su} (Fig. 10) proposed by Stevens (1987) were adopted:

$$\sigma_{sy} = \sigma_{sy}^{\exp} - 3\Delta\sigma_{ycr}\ ;\ \sigma_{sh} = \sigma_{sh}^{\exp} - \Delta\sigma_{ycr}\ ;\ \sigma_{su} = \sigma_{su}^{\exp} - \Delta\sigma_{ycr}\ ;\ \Delta\sigma_{ycr} = 75\,\phi_s / f_{ct} \quad (3)$$

being $\sigma_{sy}^{\exp}$, $\sigma_{sh}^{\exp}$ and $\sigma_{su}^{\exp}$ the values registered experimentally, f_{ct} is the concrete tensile strength in MPa and ϕ_s is the bar diameter (or equivalent bar diameter) in mm. The values in Table 9 are already affected by these reduction factors. The CFRP laminates were assumed as an isotropic material of an elasticity modulus of 160 GPa and null Poisson's coefficient, since the consideration of their real orthotropic properties has marginal influence in terms of their contribution for the behaviour of NSM strengthened RC slabs.

Figures 11 to 13 compare the load-deflection curves obtained numerically and recorded experimentally for the slabs of SL15, SL30 and SL45 series, respectively. The quite good predictive performance of the model is also visible in the strains of the steel bars, concrete and CFRP strips, as Figure 14 shows. Due to lack of space only SL15s50 slab is analyzed in this work, but similar good predictive performance was obtained in the remaining slabs (Dalfré and Barros 2009).

4 HIGH EFFECTIVE NSM FLEXURAL STRENGTHENING ARRANGEMENTS

4.1 Strengthening arrangements

As Figures 4 to 6 have revealed, to increase significantly the load carrying capacity of the RC slabs the sagging zones need also to be strengthened. Using the ACI 440 (2007) recommendations, the NSM CFRP strengthening configurations for the loaded sections were designed. The CFRP strips in the sagging regions are placed according to the representation shown in Figure 15. The total length of the laminates in the sagging regions ranged from 1080 to 1460 mm, centred in the loaded section, as shown in Figures 16 to 18 (details can be found in Dalfré and Barros 2009a). The arrangement of the steel bars and the positioning of the laminates in the hogging region are the same adopted in the experimentally tested slabs. The resisting bending moments of the LS ($M_{Rd,N}^{+}$) of the slabs have now the values indicated in the last column of Table 6.

4.2 Numerical simulations

To simulate the behaviour of the these slabs, which are NSM flexural strengthened in both the hogging and sagging regions, the values of the properties of the constitutive models adopted in the simulations of the slabs tested experimentally are also used. The finite element mesh, support and load conditions are also assumed equal to those adopted in the simulations of the experimentally tested slabs.

The relationship between the load and the deflection at the loaded sections for the three series of slab strips are presented in Figure 19. It is visible that the strengthening arrangements applied in the hogging and sagging regions are very effective in terms of increasing the load carrying capacity of the three series of slabs.

Table 11 resumes the results obtained numerically when a plastic hinge formed at the sagging region (at loaded section, LS). At the yield initiation of the steel bars of the sagging regions the increase percentage of load carrying capacity provided by the used flexural strengthening arrangements are: 13% and 25% for SL15s25 and SL15s50; 12% and 24% for SL30s25 and SL30s50; 11% and 23% for SL45s25 and SL45s50. At a concrete compressive strain of 3.5‰ in the sagging regions, the increase percentage of load carrying capacity provided by the used flexural strengthening arrangements was: 39% and 71% for SL15s25 and SL15s50; 35% and 65% for SL30s25 and SL30s50; 27% and 54% for SL45s25 and SL45s50. These values reveal that the aimed increase in terms of slab's load carrying capacity was attained. Since the slabs have not specific reinforcements for the shear resistance, the maximum load of all simulated slabs might be limited by their out-of-plane shear resistance (as proved by a recently carried out experimental test with SL15 series (Dalfré and Barros 2009b)).

4.3 Ductility analysis

Ductility is defined as the capacity of a material, cross-section, or structure to sustain considerable plastic deformation without loss of strength capacity. When applied to RC elements, the term ductility implies the ability to sustain significant inelastic deformation prior to collapse. As the evolving technology of using CFRP laminates for strengthening RC structures has attracted much attention in recent years, understanding the effects of such materials on the ductility of RC members is an important aspect on the structural performance of the FRP-strengthened structure. A method, based on the ductility index commonly used, is herein considered to analyze the ductility of the RC elements strengthened in both the hogging and sagging regions.

Ductility of RC members has generally been measured by parameters designated as bending ductility indexes. In this work, the displacement and curvature ductility of the numerically analyzed slabs strips are compared. Displacement ductility index, μ_{Δ}^{LS}, is defined as the ratio between the deflection at LS at the ultimate condition (Δ_u^{LS}) and the deflection at the yielding of the tension reinforcement at the loaded section (Δ_y^{LS}):

$$\mu_{\Delta}^{LS} = \frac{\Delta_u^{LS}}{\Delta_y^{LS}} \tag{4}$$

The curvature ductility index, μ_{χ}^{LS}, is defined as the ratio between the curvature at LS at the ultimate condition (χ_u^{LS}) and the curvature at the yielding of the tension reinforcement at loaded section (χ_y^{LS}):

$$\mu_{\chi}^{LS} = \frac{\chi_u^{LS}}{\chi_y^{LS}} \quad (5)$$

The deflection and the curvature at ultimate condition (Δ_u^{LS} and χ_u^{LS}) were obtained when a compressive strain of 3.5 ‰ was attained in the concrete surface at loaded section.

Table 12 lists the values of the ductility indexes obtained for the three series of slabs. It is worth noting that:

(i) When compared to the reference slabs of the tested series, the increase of Δ_u^{LS} in the strengthened slabs was larger than the increase of Δ_y^{LS}, resulting μ_{Δ}^{LS} values that are higher in these later slabs than in the former ones. However, this deflection ductility performance has decreased with the increase of $\rho_{l,eq}$ (Table 10), where $\rho_{l,eq} = A_{sl}/(bd_s) + (A_f E_f/E_s)/(bd_f)$ is the equivalent reinforcement ratio provided by both tensile steel bars and NSM laminates.

(ii) The ductility index should exceed a minimum value to ensure that the internal reinforcement experiences plastic deformation and to prevent the occurrence of sudden failure in the strengthened flexural members. According to the *fib* recommendations (2001), the minimum ductility index, in terms of curvature, should be 1.7 for structures of concrete strength class lower of equal to C35/40, and 2.6 for structures of concrete strength class higher than C35/40. The values of the ductility curvature index for the tested continuous slab strips strengthened with CFRP laminates range from 2.60 to 4.52, therefore the aforementioned ductility requirement is accomplished.

(iii) In terms of curvature ductility a decrease of χ_u^{LS} with the increase of $\rho_{l,eq}$ at the sagging region was obtained, which resulted in a decrease of μ_{χ}^{LS}.

(iv) The graphs of Figure 20 show the relationship between the applied load and the moment redistribution percentage, η, for the three series of slab strips numerically analyzed. At the formation of the plastic hinge in the sagging region the following η values were obtained: 10.1%, 6.2% and 3.7% for SL15, SL15s25, SL15s50; 22.4%, 17.8% and 14.5% for SL30, SL30s25, SL30s50, 40.2%, 36.6% and 31.8% for SL45, SL45s25 and SL45s50. For a compressive strain of 3.5 ‰ in the concrete surface at loaded sections, the following η values were obtained: 11.7%, 7.1% and 5.0% for SL15, SL15s25 and SL15s50; 26.0%, 20.7% and 17.3% for SL30, SL30s25 and SL30s50; 41.0%, 38.2% and 32.9% for SL45, SL45s25 and SL45s50.

6. CONCLUSIONS

In a recent PhD thesis dealing with the NSM flexural strengthening of continuous RC slabs the author reported an effectiveness of this technique lower than as expected in term of increasing the load carrying and the moment

redistribution capacities. This experimental program was analysed in depth in the present paper and it was concluded that deficient flexural strengthening arrangements were applied in the strengthened slabs, justifying the lack of effectiveness of the NSM technique for this type of structures.

Using the obtained experimental results, the capability of a FEM-based computer program to predict with high accuracy the behaviour of this type of structures up to its collapse was highlighted. Using this program, the high effectiveness of this technique for the increase of the load carrying capacity was attested when correct NSM flexural strengthening arrangements are used. Additionally, if the NSM strengthening system is designed properly and precautions are taken to prevent shear or debonding failure, relevant moment redistribution levels can occur along the strengthened elements up to their final failure.

7. ACKNOWLEDGEMENTS

The study reported in this paper forms a part of the research program "CUTINEMO - Carbon fiber laminates applied according to the near surface mounted technique to increase the flexural resistance to negative moments of continuous reinforced concrete structures" supported by FCT, PTDC/ECM/73099/2006. The authors wish to acknowledge the support also provided by the S&P, Casais and Artecanter Companies. The first Author acknowledges the financial support of National Council for Scientific and Technological Development (CNPq) – Brazil, Ph.D. Grant no. 200953/2007-9. The second Author wishes to acknowledge the support provided by FCT, by means of the SFRH/BSAB/818/2008 and SFRH/BSAB/913/2009 sabbatical grants.

REFERENCES

ACI Committee 318. (2004). *ACI 318-04 - Building code requirements for structural concrete and Commentary*, American Concrete Institute, Detroit.

ACI Committee 440. (2007). *ACI 440 - Guide for the design and construction of externally bonded FRP systems for strengthening concrete structures*, American Concrete Institute.

Arduini, M., Tommaso, D. A. and Nanni, A. (1997). "Brittle Failure in FRP Plate and Sheet Bonded Beams", *ACI Structural Journal*, 94 (4), pp. 363-370.

Ashour, S.A. (2000). "Effect of compressive strength and tensile reinforcement ratio on flexural behavior of high-strength concrete beams", *Engineering Structures*, Vol. 22, pp. 413-423.

Ashour, A. F., El-Rafaie, S. A. and Garrity, S. W. (2004). "Flexural strengthening of RC continuous beams using CFRP laminates", *Cement and Concrete Composites*, No. 26, pp. 765-775.

ASTM 370. (2002). *Standard test methods and definitions for mechanical testing of steel products*, American Society for Testing and Materials.

ASTM D3039. (1993). Standard *test method for tensile properties of polymer matrix composite materials*, American Society for Testing and Materials, Annual Book of ASTM Standards, Vol. 15.03, pp. 118-127, West Conshohocken, PA.

Barros, J.A.O., Dalfré, G.M. and Dias, J.P. (2008). "Numerical Simulation of Continuous RC Slabs Strengthened using NSM Technique*", Proceedings of 2nd International Conference on Concrete Repair, Rehabilitation and Retrofitting*, Cape Town, South Africa, November.

Barros, J.A.O. and Fortes, A.S. (2005). "Flexural strengthening of concrete beams with CFRP laminates bonded into slits", Journal *Cement and Concrete Composites*, Vol. 27(4), pp. 471-480.

Barros, J.A.O., Dias, S.J.E. and Lima, J.L.T. (2007). "Efficacy of CFRP-based techniques for the flexural and shear strengthening of concrete beams", *Journal Cement and Concrete Composites*, Vol. 29(3), pp. 203-217.

Barros, J.A.O. and Figueiras, J.A. (2001). "Nonlinear analysis of steel fibre reinforced concrete slabs on grade", *Computers & Structures Journal*, Vol. 79(1), pp. 97-106.

Blaschko, M. and Zilch, K. (1999). "Rehabilitation of concrete structures with CFRP strips glued into slits", *Proceedings of 12th International Conference on Composite Materials*, Paris, France, July.

Bonaldo, E. (2008). *Composite materials and discrete steel fibres for the strengthening of thin concrete structures*, PhD Thesis, University of Minho, Guimarães, Portugal.

Bonaldo, E., Barros, J.A.O. and Lourenço, P.J.B. (2008). "Efficient strengthening technique to increase the flexural resistance of existing RC slabs", *Journal of Composites for Construction, Vol.* 12(2), pp. 149-159.

Casadei, P., Nanni, A., Galati, N., Ibell, T. and Denton, S. (2003). "Moment redistribution in continuous CFRP-strengthened concrete members: experimental results", *Proceedings of International Conference Composites in Construction - CCC2003*, Cosenza, Italy, September.

CEB-FIP Model Code 1990. (1993). *Design Code*. Thomas Telford, Lausanne, Switzerland.

Concrete Society (2000). *Design guidance for strengthening concrete structures using fibre composite materials*, Concrete Society Technical Report No 55, The Concrete Society, Century House, Telford Avenue, Crowthorne, Berkshire, UK.

Dalfré, G.M. and Barros, J.A.O. (2009a). *Numerical analysis of two-way RC slabs flexural strengthened with NSM CFRP laminates*, Technical Report 09-DEC/E-09, Dep. Civil Eng., School Eng. University of Minho, 90 pags.

Dalfré, G.M. and Barros, J.A.O. (2009b). "*Movies of the SL15s25 slab of the second group of the NSM flexural strengthened continuous RC slabs*". (http://www.civil.uminho.pt/mrtest)

El-Hacha, R. and Rizkalla, S.H. (2004). "Near-surface-mounted fiber-reinforced polymer reinforcements for flexural strengthening of concrete structures", *ACI Structural Journal*, Vol. 101(5), pp. 717-726.

El-Refaie S.A., Ashour A.F. and Garrity, S.W. (2003a). "Sagging and hogging strengthening of continuous reinforced concrete beams using CFRP sheets", *ACI Structural Journal*, Vol. 100, No. 4, July-August, pp. 446-453.

El-Refaie S. A., Ashour A. F. and Garrity, S. W. (2003b). "CFRP strengthened continuous concrete beams", *Structures and Buildings*, Vol. 156, No. 4, November, pp. 395-404.

EN 1992-1-1 (2004). "*Eurocode 2: Design of Concrete Structures-Part 1-1: General Rules and Rules for Buildings*", CEN, Brussels, December.

Fédération Internationale du Béton (FIB). (2001). *Externally bonded FRP reinforcement for RC structures*, Bulletin 14, Lausanne, Switzerland.

Hassan, T. and Rizkalla, S. (2003). "Investigation of bond in concrete structures strengthened with near surface mounted carbon fiber reinforced polymer strips", *Journal of Composites for Construction*, Vol. 07, No. 03, pp. 248-257.

ISO 527-1. (1993). *Plastics - Determination of tensile properties - Part 1: General principles*, International Organization for Standardization (ISO), Genèva, Switzerland, 9 pp.

ISO 527-5 (1993). *Plastics - Determination of tensile properties - Part 5: Test conditions for unidirectional fibre-reinforced plastic composites*, International Organization for Standardization (ISO), Genèva, Switzerland, 9 pp.

Kotynia, R. (2006). "Analysis of reinforced concrete beams strengthened with near surface mounted FRP reinforcement", *Archives of Civil Engineering*, LII 2, 305-317.

Liu, I.S.T., Oehlers, D.J., Seracino, R. and Ju, G. (2006a). "Moment redistribution parametric study of CFRP, GFRP and steel surface plated RC beams and slabs", *Construction and Building Materials*, No. 20, pp. 59-70.

Liu, I. S. T., Oehlers, D. J. and Seracino, R. (2006b). "Tests on the ductility of reinforced concrete beams retrofitted with FRP and steel near-surface mounted plates", *Journal of Composites for Construction*, Vol. 10, No. 02.

Nanni, A., Di Ludovico, M. and Parretti, R. (2004). "Shear strengthening of a PC bridge girder with NSM CFRP rectangular bars", *Advances in Structural Engineering*, 7(4), 97-109.

Oehlers, D.J., Campbell, L., Haskett, M., Antram, P. and Byrne, R. (2006). "Moment redistribution in RC beams retrofitted by longitudinal plating", *Advances in Structural Engineering*, Vol. 9, No. 2, April, pp. 257-264.

Oehlers, D.J., Ju, G., Liu, I.S.T. and Seracino, R. (2004a). "Moment redistribution in continuous plated RC flexural members. Part1: neutral axis depth approach and tests", *Engineering Structures*, No. 26, pp. 2197-2207.

Oehlers, D.J., Liu, I.S.T., Ju, G. and Seracino, R. (2004b). "Moment redistribution in continuous plated RC flexural members. Part2: Flexural rigidity approach", *Engineering Structures*, No. 26, pp. 2209-2218.

Park, S. M. and Oehlers, D. J. (2000). *Details of tests on steel and FRP plated continuous reinforced concrete beams*, Research Report R170, School of Civil and Environmental Engineering, University of Adelaide.

Sena-Cruz, J.M. (2004). *Strengthening of concrete structures with near-surface mounted CFRP laminate strips*, PhD Thesis, Department of Civil Engineering, University of Minho, Guimarães, Portugal. http://www.civil.uminho.pt/composites, 2004

Stevens, N. J. (1987). *Analytical modelling of reinforced concrete subjected to monotonic and reversed loadings*, Publication No. 87-1, ISBN 0-7727-7088-3, University of Toronto, January.

Täljsten, B., Carolin, A. and Nordin, H. (2003). "Concrete structures strengthened with near surface mounted reinforcement of CFRP", *Advances in Structural Engineering*, Vol. 06, No. 03, August, pp. 201-213.

NOTATION

Roman upper case letters

A_c	=	cross-sectional area of concrete
A_s`		Cross-sectional area of the longitudinal tensile steel bars placed at top reinforcement
A_s		Cross-sectional area of the longitudinal tensile steel bars placed at bottom reinforcement
A_f	=	cross-sectional area of CFRP laminates
$\mathrm{M_{red}}$	=	moment in the critical section after redistribution
$\mathrm{M_{elas}}$	=	the elastic moment calculated according to the theory of elasticity
F	=	point load
M^-_{Exp}	=	experimental negative bending moment
$\overline{F}_{\max}$	=	maximum value of the average of the forces applied in the two spans
$\overline{R}_{L,\overline{F}_{\max}}$	=	reactions at external support at $\overline{F}_{,max}$
$\overline{R}_{C,\overline{F}_{\max}}$	=	reactions at central supports at $\overline{F}_{,max}$
M^+_{static}	=	moment at loaded section obtained by static equilibrium
M^-_{static}	=	moment at intermediate support obtained by static equilibrium
$\overline{\mathrm{F}}_{\mathrm{y}}^{\mathrm{IS}}$	=	average loads at the formation of the plastic hinge at IS
$\overline{\mathrm{F}}_{\mathrm{y}}^{\mathrm{LS}}$	=	average loads at the formation of the plastic hinge at LS
$\mathrm{F_{max}}$	=	maximum load up to a concrete compressive strain of 3.5‰
$\overline{\mathrm{F}}_{\mathrm{cr}}$	=	cracking load
M^+_{Rd}	=	positive resisting-bending moments
M^-_{Rd}	=	negative resisting-bending moments
$\overline{F}$	=	Average load

Greek lower case letters

δ	=	coefficient of moment redistribution
η	=	moment redistribution percentage
ε_{fd}	=	CFRP laminate strain

ε_{fu}	=	ultimate CFRP laminate strain
$\varepsilon_{c,max}^{IS}$, $\varepsilon_{c,max}^{LS}$	=	maximum concrete strains at IS and LS, respectively
$\varepsilon_{s,max}^{LS}$, $\varepsilon_{s,max}^{IS}$	=	maximum strains in steel bars at IS and LS, respectively
$\varepsilon_{f,max}$	=	maximum strain in the CFRP laminates
$\varepsilon_{f,max}^{Fmax}$	=	maximum strain in the CFRP laminates at F_{max}
$\varepsilon_{s,max}^{Fmax}$	=	maximum strain in steel bars at F_{max}
χ_y	=	curvature at the formation of the hinge at intermediate support
u_y^{IS}	=	deflection at the formation of the plastic hinge at IS
u_y^{LS}	=	deflection at the formation of the plastic hinge at LS
$\varepsilon_{f,max}^{\bar{F}}$, $\varepsilon_{s,max}^{\bar{F}}$	=	Maximum strain in the CFRP laminates and in steel bars at $\bar{F}$.
$\rho_{l,eq}$	=	Equivalent reinforcement ratio

Greek upper case letters

ΔM_{Tar}^{-}	=	target increase of negative resisting bending moment
ΔM^{-}	=	variation of negative bending moment
ΔF	=	variation of applied load
Δ_y		Deflection at the formation of the hinge at intermediate support

LIST OF TABLE CAPTIONS

Table 1 – Geometry, reinforcement and strengthening details of the cross sections of the slab strips.

η	M^- increasing	Cross-Section S_1-S_1'	Cross-Section S_2-S_2'	Number of CFRP laminates	$\rho_{l,eq}$ (%)
15%	Reference	A_s' = 2ϕ12mm A_s = 4ϕ12mm + 3ϕ8mm	A_s = 5ϕ12mm A_s' = 2ϕ12mm + 1ϕ8mm	0	1.604
	25%			3	1.677
	50%			7	1.775
30%	Reference	A_s' = 2ϕ12mm A_s = 3ϕ12mm + 4ϕ10mm	A_s = 4ϕ12mm A_s' = 2ϕ10mm + 1ϕ12mm	0	1.283
	25%			2	1.332
	50%			5	1.405
45%	Reference	A_s' = 2ϕ10mm A_s = 6ϕ12mm + 1ϕ8mm	A_s = 3ϕ10mm + 2ϕ8mm A_s' = 2ϕ12mm + 1ϕ8mm	0	0.954
	25%			1	0.978
	50%			3	1.027

Table 2 – Concrete average compressive strength.

Age	f_{cm} (MPa)		
	SL15	SL30	SL45
At 28 days	40.07 (0.59)	35.99 (0.51)	41.41 (0.22)
At the slabs testing age	44.38 (1.06) [126]	44.91 (1.33) [105]	49.29 (1.76) [204]

(value) Standard deviation
[value] Slab testing age (days)

Table 3 – Mechanical properties of the steel bars.

Steel bar diameter (mm)	Modulus of elasticity (kN/mm^2)	Yield stress (0.2 %)[a] (N/mm^2)	Strain at yield stress[b]	Tensile strength (N/mm^2)
6	193.80 (10.89) [5.62%]	447.66 (2.81) [0.63%]	0.0025 (0.0001) [4.68%]	566.66 (3.53) [0.62%]
8	200.80 (4.69) [2.33%]	421.35 (2.25) [0.53%]	0.0023 (0.0001) [2.65%]	578.75 (2.09) [0.36%]
10	178.24 (4.42) [2.48%]	446.95 (14.55) [3.26%]	0.0027 (0.0000) [0.45%]	575.95 (1.94) [0.34%]
12	198.36 (5.49) [2.77%]	442.47 (12.68) [2.87%]	0.0024 (0.0000) [0.19%]	539.88 (9.93) [1.84%]

[a] Yield stress determined by the "Offset Method", according to ASTM 370 (2002)
[b] Strain at yield point, for the 0.2 % offset stress
(value) Standard deviation
[value] Coefficient of Variation (COV) = (Standard deviation/Average) × 100

Table 4 – CFRP laminates properties.

Ultimate	Ultimate	Modulus of	Modulus of

tensile stress (N/mm^2)	tensile strain (‰)	elasticity[a] (kN/mm^2)	elasticity[b] (kN/mm^2)
2867.63	17.67	159.30	164.90
(88.10)	(0.54)	(5.01)	(2.29)
[3.07%]	[3.04%]	[3.15%]	[1.39%]

[a] According to ISO 527-1 and ISO 527-5 (1993)
[b] Tensile Chord Modulus of Elasticity, according to ACI 440 (2007) and ASTM D3039 (1993)
(value) Standard deviation
[*value*] Coefficient of Variation (COV) = (Standard deviation/Average) × 100

Table 5 – Main results.

Slab reference	ΔM^-_{Tar} (%)	$\bar{F}_{max}$ (kN)	$\bar{R}_{L,\bar{F}max}$ (kN)	$\bar{R}_{C,\bar{F}max}$ (kN)	ΔM^-_{Exp} (kN.m)
SL15	-	51.36	17.66	67.39	22.46
SL15S25	25	57.60 (12.15%)	16.70	81.80	33.88 (50.84%)
SL15S50	50	62.36 (21.42%)	17.46	89.79	38.42 (71.06%)
SL30	-	49.84	19.12	61.44	16.24
SL30S25	25	54.87 (10.09%)	18.92	71.91	23.84 (46.80%)
SL30S50	50	58.09 (16.55%)	18.74	78.70	28.85 (77.64%)
SL45	-	52.55	21.63	61.85	13.01
SL45S25	25	54.49 (3.69%)	20.94	67.10	17.65 (35.66%)
SL45S50	50	57.79 (9.97%)	20.82	73.94	22.61 (73.79%)

Table 6 – Elastic redistribution of bending moments and the corresponding variation of the applied load for the series of slabs.

	M^+_{static} (kN.m)	M^-_{static} (kN.m)	ΔM^- (kN.m)	ΔF (kN)	F (kN)	M^+_{Rd} (kN.m)	M^-_{Rd} [(1)] (kN.m)	ΔM^-_{Rd} [(2)] (kN.m)	$M^+_{Rd,N}$ [(3)] (kN.m)
SL	22.24	26.68	-----	-----	50.82	-----	-----	-----	-----
SL15	24.24	22.68	-----	-----	50.82	25.16	-----	-----	25.16
SL15s25	30.29	28.35	5.67	12.71	63.53	25.16	30.41	7.73	31.70
SL15s50	36.35	34.02	11.34	25.41	76.23	25.16	38.70	16.02	39.87
SL30	26.23	18.68	-----	-----	50.82	26.97	-----	-----	26.97
SL30s25	32.79	23.35	4.67	12.71	63.53	26.97	24.12	5.44	35.44
SL3050	39.35	28.02	9.34	25.41	76.23	26.97	30.80	12.12	41.38
SL45	28.23	14.68	-----	-----	50.82	29.60	-----	-----	29.60
SL45s25	35.29	18.35	3.67	12.70	63.53	29.60	19.66	4.98	37.82
SL45s50	42.35	22.02	7.34	25.41	76.23	29.60	24.34	9.66	45.41

[(1)] Obtained using the formulation proposed by ACI 440; [(2)] $\Delta M^-_{Rd} = M^-_{Rd} - M^-_{static}$; [(3)] slabs strengthened in both sagging and hogging regions.

Table 7 – Main results – Experimental program.

	Series	Hinge at hogging region (IS)							Hinge at sagging region (LS)							ε_c^{IS} (-3.5‰)		
		$\bar{F}_y^{IS}$ (kN)	$\bar{u}_y^{IS}$ (mm)	$\varepsilon_{c,max}^{IS}$ (‰)	$\varepsilon_{c,max}^{LS}$ (‰)	$\varepsilon_{s,max}^{LS}$ (‰)	$\varepsilon_{s,max}^{IS}$ (‰)	$\varepsilon_{f,max}$ (‰)	$\bar{F}_y^{LS}$ (kN)	$\bar{u}_y^{IS}$ (mm)	$\varepsilon_{c,max}^{IS}$ (‰)	$\varepsilon_{c,max}^{LS}$ (‰)	$\varepsilon_{s,max}^{LS}$ (‰)	$\varepsilon_{s,max}^{IS}$ (‰)	$\varepsilon_{f,max}$ (‰)	$\bar{F}$ (kN)	$\varepsilon_{f,max}^{\bar{F}}$ (‰)	$\varepsilon_{s,max}^{\bar{F}}$ (‰)
SL15	Reference	42.67	15.86	-1.38	-1.13	2.04	2.40	-----	46.99	19.80	-1.71	-1.38	2.45	2.91	-----	49.22	-----	2.46
	SL15s25	49.13	18.52	-1.74	-1.29	2.32	2.42	3.19	51.36	20.09	-1.93	-1.60	2.40	2.73	3.47	53.17	7.82	2.87
	SL15s50	54.33	21.77	-1.97	-1.48	2.70	2.41	4.06	54.38	19.67	-1.71	-1.31	2.40	2.21	3.36	58.95	7.64	2.75
SL30	Reference	31.52	11.82	-1.15	-0.90	1.32	2.40	-----	48.48	24.07	-3.38	-1.82	2.70	4.38	-----	48.51	-----	4.44
	SL30s25	43.66	17.63	-1.54	-1.25	1.78	2.30	2.77	49.90	24.98	-2.80	-1.77	2.50	2.60	5.90	51.39	7.35	2.64
	SL30s50	42.39	16.26	-1.83	-1.31	2.17	2.40	4.13	51.96	21.63	-2.70	-1.76	2.77	2.74	6.25	52.95	8.13	2.88
SL45	Reference	32.50	12.16	-1.01	-0.97	1.15	m.d.	-----	50.20	27.88	-4.05	-2.11	2.77	m.d.	-----	50.89	-----	0.80
	SL45s25	33.59	12.27	-1.08	-0.86	1.11	m.d.	2.97	53.42	33.57	-5.15	-3.54	2.40	2.38	11.95	52.35	9.65	1.66
	SL45s50	38.00	14.45	-1.22	-1.06	1.62	m.d.	2.93	53.00	23.19	-2.35	-1.64	2.40	1.78	6.44	55.20	9.34	2.12

m.d.: The gauge may have been mechanically damaged

Table 8 - Values of the parameters of the concrete constitutive model.

Poisson's ratio	$\nu_c = 0.15$
Initial Young's modulus	$E_c = 28000$ N/mm^2
Compressive strength	$f_c = 40$ N/mm^2
Strain at peak compression stress	$\varepsilon_{c1} = 2.2\text{x}10^{-3}$
Parameter defining the initial yield surface (Sena-Cruz 2004)	$\alpha_0 = 0.4$
Trilinear tension softening/stiffening diagram [(1)]	$f_{ct} = 1.5$ N/mm^2 ; $G_f = 0.05$ N/mm $\xi_1 = 0.015$; $\alpha_1 = 0.6$; $\xi_2 = 0.2$; $\alpha_2 = 0.25$
Parameter defining the mode I fracture energy available to the new crack (Sena-Cruz 2004)	$n = 2$
Parameter for defining the shear retention factor (Sena-Cruz 2004)	$p_1 = 2$
Crack band-width, l_b	*Square root of the area of Gauss integration point*
Threshold angle (Sena-Cruz 2004)	$\alpha_{th} = 30^o$
Maximum number of cracks per integration point	2

[(1)] $f_{ct} = \sigma_{n,1}^{cr}$; $\xi_1 = \varepsilon_{n,2}^{cr} / \varepsilon_{n,u}^{cr}$; $\alpha_1 = \sigma_{n,2}^{cr} / \sigma_{n,1}^{cr}$; $\xi_2 = \varepsilon_{n,3}^{cr} / \varepsilon_{n,u}^{cr}$; $\alpha_2 = \sigma_{n,3}^{cr} / \sigma_{n,1}^{cr}$ (see Figure 9)

Table 9 – Values of the parameters of the steel constitutive model (see Figure 10).

Steel bar diameter	$P_1(\varepsilon_{sy}[-];\sigma_{sy}[MPa])$	$P_2(\varepsilon_{sh}[-];\sigma_{sh}[MPa])$	$P_3(\varepsilon_{su}[-];\sigma_{su}[MPa])$	E_s [GPa]
∅ 8mm	$(1.90x10^{-3}; 379.16)$	$(4.42x10^{-2}; 512.19)$	$(8.85x10^{-2}; 541.66)$	200.80
∅ 10mm	$(2.32x10^{-3}; 413.20)$	$(3.07x10^{-2}; 434.75)$	$(1.31x10^{-1}; 546.25)$	178.24
∅ 12mm	$(2.09x10^{-3}; 414.35)$	$(3.05x10^{-2}; 435.63)$	$(1.02x10^{-1}; 537.98)$	198.36

Table 10 – Mechanical properties of the materials.

CFRP Laminate Strips	
Properties	MBrace Laminate LM
f_{fu}^*	2740 MPa
E_f	160 GPa
ε_{fu}^*	17.12 ‰
b_f	1.4 mm
h_f	9.4 mm

Table 11 – Results obtained numerically at LS.

	Series	Hinge at sagging region (LS)			ε_c^{LS} (-3.5‰)				Laminate Strips			
		F_y^{LS} (kN)	ε_s^{LS} (‰)	$\frac{F_y^{LS}}{F_{y,ref}^{LS}}$ (%)	F (kN)	ΔF (kN)	ε_s (‰)	$\frac{F}{F_{ref}}$ (%)	S1-S1	$\rho_{l,eq}$ (%)	S2-S2	$\rho_{l,eq}$ (%)
SL15	Reference	44.44	2.37	------	47.55	------	13.27	------	------	1.71	------	1.60
	SL15s25	50.40	2.60	13.41	66.23	18.68	10.15	39.28	3	1.78	3	1.68
	SL15s50	55.61	2.11	25.13	81.53	33.98	7.76	71.46	7	1.88	7	1.77
SL30	Reference	44.02	2.17	------	47.42	------	12.20	------	------	1.85	------	1.28
	SL30s25	49.32	2.20	12.04	63.86	16.44	9.50	34.67	3	1.93	2	1.33
	SL30s50	54.70	2.14	24.26	78.30	30.88	7.50	65.12	7	2.02	5	1.41
SL45	Reference	45.85	2.10	------	48.40	------	11.38	------	------	2.07	------	0.95
	SL45s25	50.91	2.45	11.03	61.28	12.88	8.19	26.61	3	2.14	1	0.98
	SL45s50	56.63	2.29	23.51	74.32	25.92	6.74	53.55	7	2.24	3	1.03

Table 12 – Ductility indexes.

	Series	Hinge at sagging region (LS)								
		F_y^{LS} (kN)	Δ_u^{LS} (mm)	Δ_y^{LS} (mm)	μ_Δ^{LS}	Increase over reference slab (%)	χ_u^{LS} ($\times 10^{-6}$)	χ_y^{LS} ($\times 10^{-6}$)	μ_χ^{LS}	Decrease over reference slab (%)
SL15	Reference	44.44	29.56	17.41	1.69	-----	173.38	38.79	4.47	-----
	SL15s25	50.40	42.22	18.01	2.34	38.46	145.19	42.74	3.40	23.94
	SL15s50	55.61	41.98	18.01	2.33	37.87	119.76	37.30	3.21	28.19
SL30	Reference	44.02	29.51	18.83	1.57	-----	166.51	36.84	4.52	-----
	SL30s25	49.31	40.62	19.01	2.14	36.30	138.25	38.14	3.62	19.91
	SL30s50	54.70	41.12	19.01	2.16	37.58	117.04	38.21	3.06	32.30
SL45	Reference	45.85	32.51	21.11	1.54	-----	158.28	37.71	4.20	-----
	SL45s25	50.91	39.95	22.02	1.81	17.53	124.51	43.60	2.86	31.90
	SL45s50	56.63	41.09	22.02	1.86	20.78	109.95	42.25	2.60	38.09

LIST OF FIGURE CAPTIONS

Figure 1 - Characteristics of the slab specimens: (a) longitudinal view of the reinforcement arrangements; reinforcement and strengthening details of the (b) SL15, (c) SL30, and (d) SL45 series; (e) geometry of the slit and CFRP strip (A_s' - top reinforcement; As – bottom reinforcement; dimensions in mm).

Figure 2 – Positioning of the (a) LVDTs, (b)-(c) strain gauges in steel bars, (d) concrete, (e)-(f) CFRP strips of the two strengthened slabs of the SL15 series (dimensions in mm).

Figure 3 – Force versus deflection at the loaded sections for the series: (a) SL15, (b) SL30, and (c) SL45.

Figure 4 – Elastic bending moments of SL15 series: (a) SL15, (b) SL15s25, (c) SL15s50.

Figure 5 – Elastic bending moments of SL30 series: (a) SL30, (b) SL30s25, (c) SL30s50.

Figure 6 – Elastic bending moments of SL45 series: (a) SL45, (b) SL45s25, (c) SL45s50.

Figure 7 - Degree of moment redistribution, η, for the slab strips series: (a) SL15, (b) SL30, (c) SL45.

Figure 8 – Finite element mesh adopted to discretize the half part of a RC slab.

Figure 9 – Crack normal stress *vs* crack normal strain diagram for modelling the concrete tensile-softening behaviour.

Figure 10 - Uniaxial constitutive model of the rebars.

Figure 11 - Force-deflection relationship for the slabs: (a) SL15, (b) SL15s25, (c) SL15s50.

Figure 12 - Force-deflection relationship for the slabs: (a) SL30, (b) SL30s25, (c) SL30s50.

Figure 13 - Force-deflection relationship for the slabs: (a) SL45, (b) SL45s25, (c) SL45s50.

Figure 14 – SL15s50: (a) load – steel strain at slab loaded sections, (b) load – concrete strain at loaded sections, (c) load – CFRP laminate strain.

Figure 15 – Specimens cross section dimensions and arrangement of the NSM CFRP strips for the slabs: (a) SL15, (b) SL30 and (c) SL45.

Figure 16 – CFRP strips of the two strengthened slabs of the SL15 series (dimensions in mm).

Figure 17 – CFRP strips of the two strengthened slabs of the SL30 series (dimensions in mm).

Figure 18 – CFRP strips of the two strengthened slabs of the SL45 series (dimensions in mm).

Figure 19 – Load-deflection at the loaded section for the slabs strengthened for the increase of both the load carrying and moment redistribution capacity: (a) SL15, (b) SL30, and (c) SL45.

Figure 20 - Degree of moment redistribution, η, for the slab strips series strengthened in the hogging and sagging regions: (a) SL15, (b) SL30, (c) SL45.

FIGURE CAPTIONS

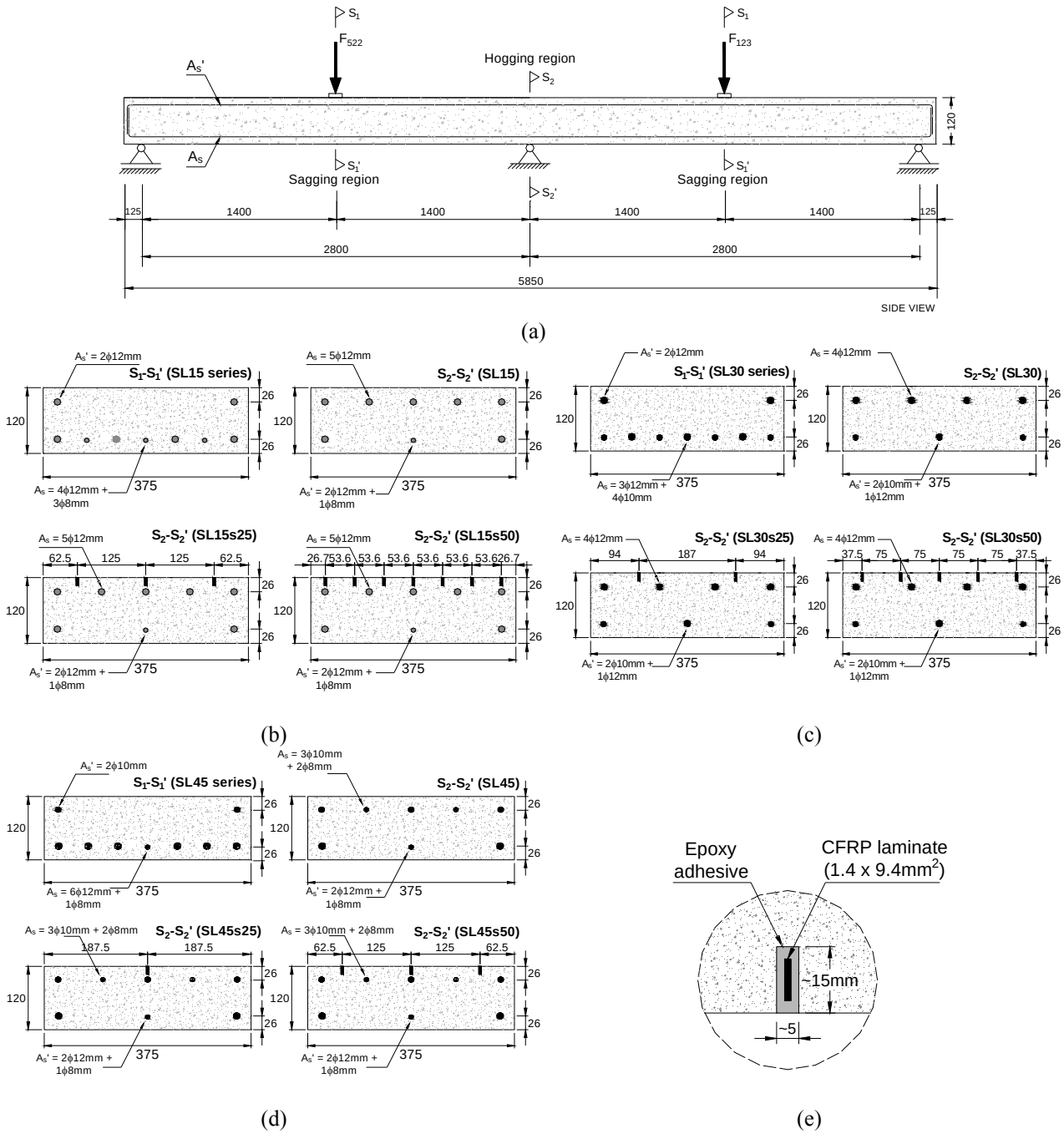

Figure 1 - Characteristics of the slab specimens: (a) longitudinal view of the reinforcement arrangements; reinforcement and strengthening details of the (b) SL15, (c) SL30, and (d) SL45 series; (e) geometry of the slit and CFRP strip ($A_s^{'}$ - top reinforcement; A_s – bottom reinforcement; dimensions in mm).

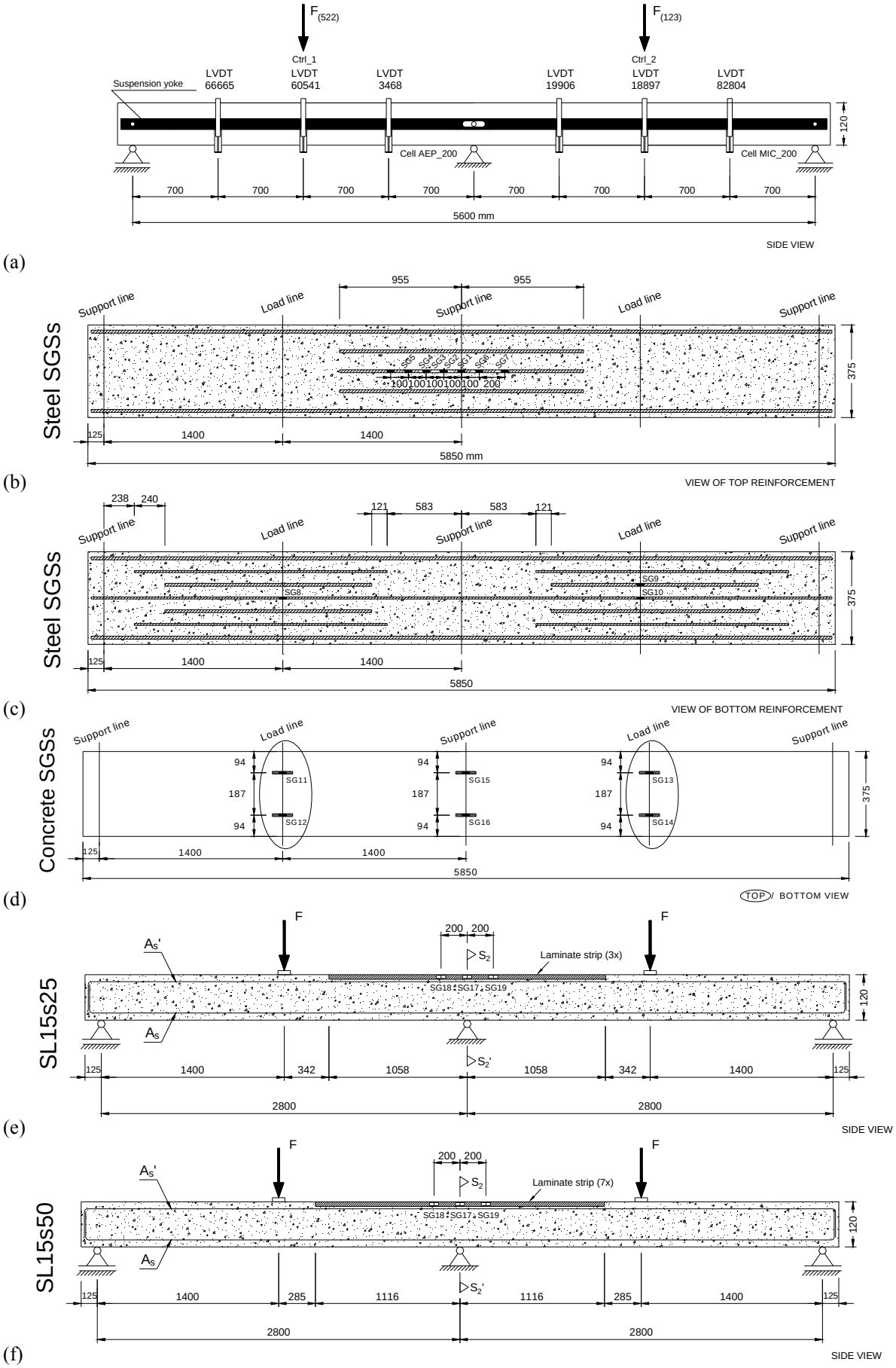

Figure 2 – Positioning of the (a) LVDTs, (b)-(c) strain gauges in steel bars, (d) concrete, (e)-(f) CFRP strips of the two strengthened slabs of the SL15 series (dimensions in mm).

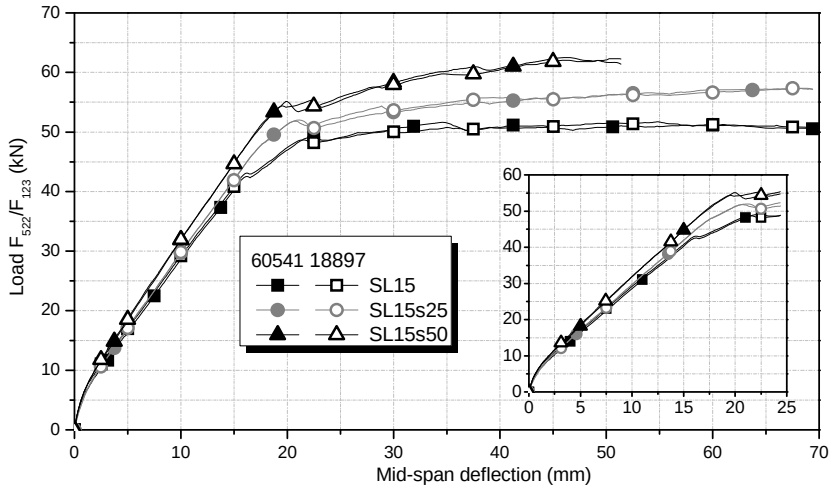

(a)

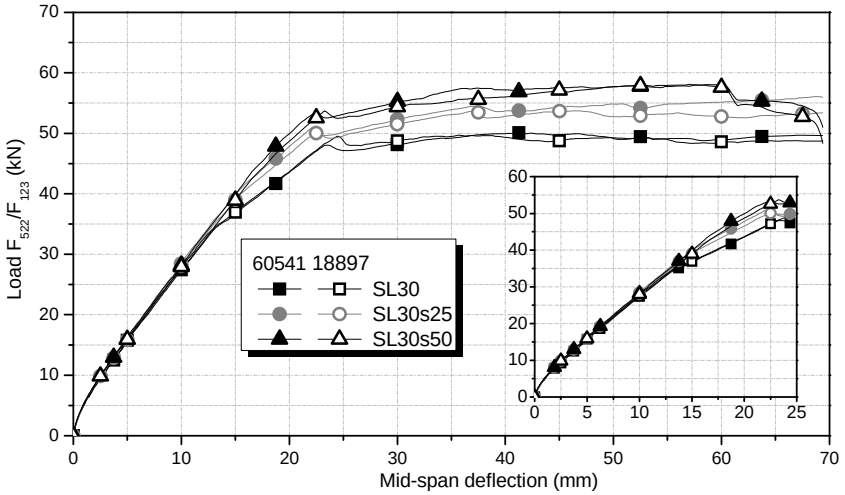

(b)

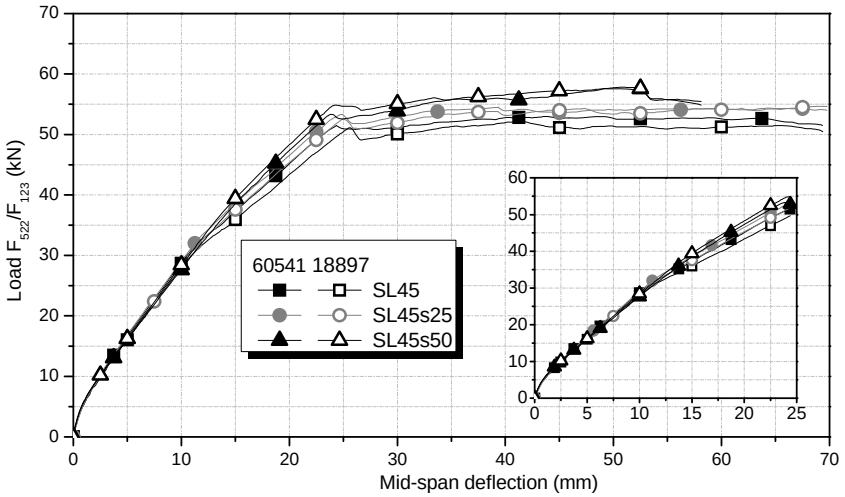

(c)

Figure 3 – Force versus deflection at the loaded sections for the series: (a) SL15, (b) SL30, and (c) SL45.

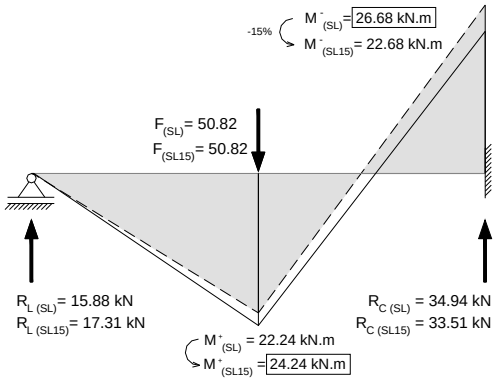

(a)

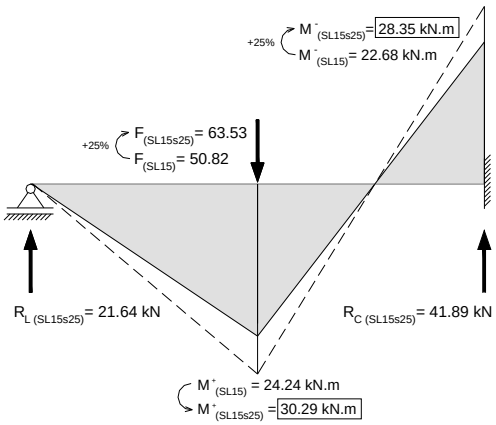

(b)

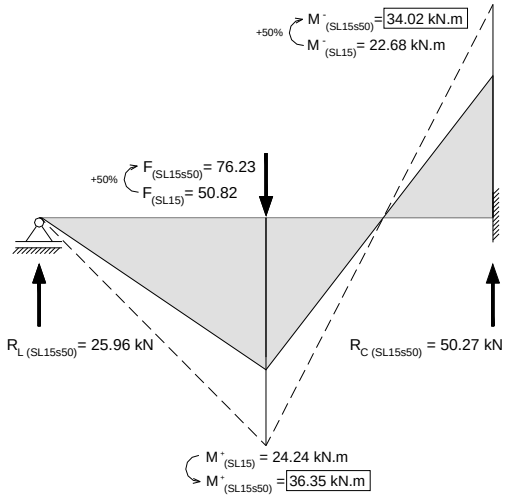

(c)

Figure 4 – Elastic bending moments of SL15 series: (a) SL15, (b) SL15s25, (c) SL15s50.

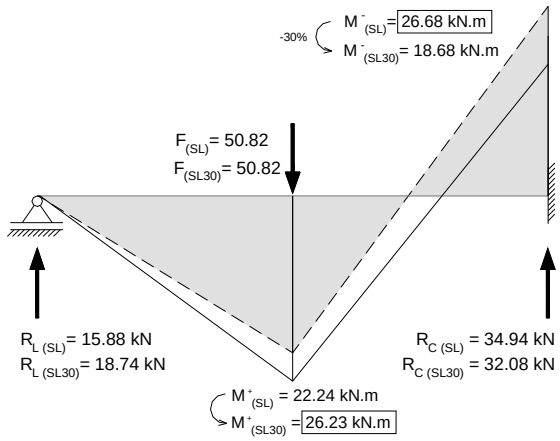

(a)

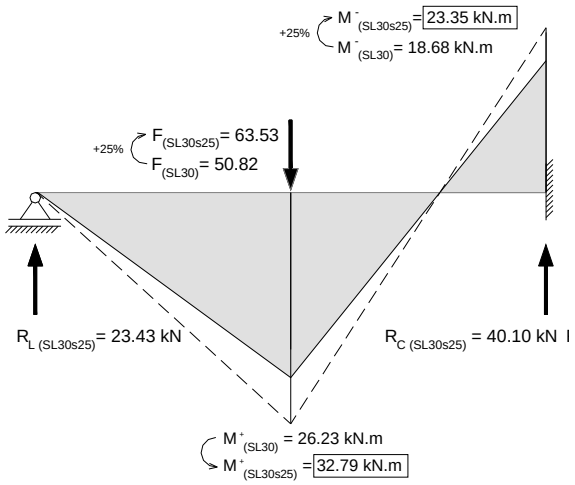

(b)

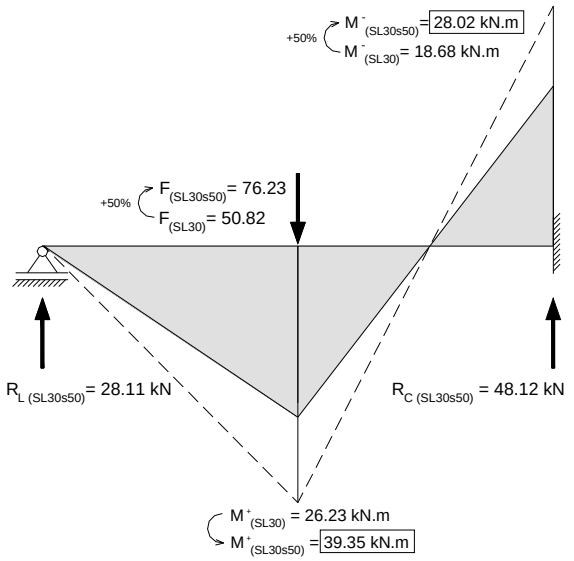

(c)

Figure 5 – Elastic bending moments of SL30 series: (a) SL30, (b) SL30s25, (c) SL30s50.

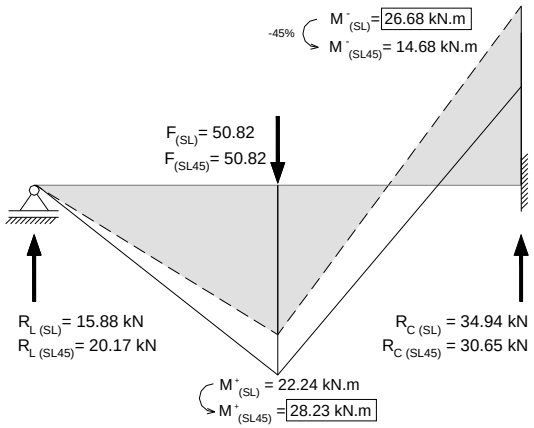

(a)

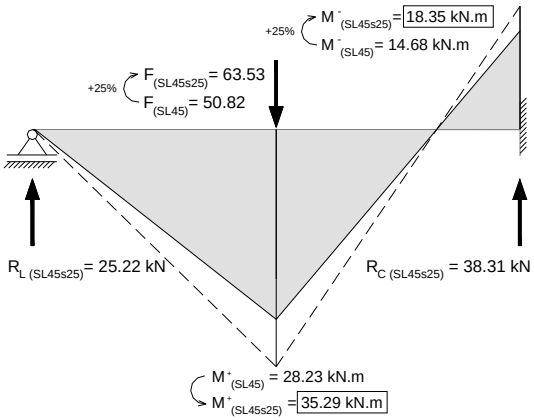

(b)

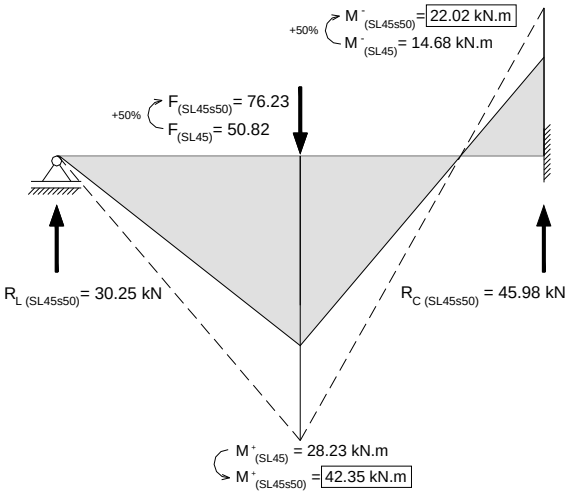

(c)

Figure 6 – Elastic bending moments of SL45 series: (a) SL45, (b) SL45s25, (c) SL45s50.

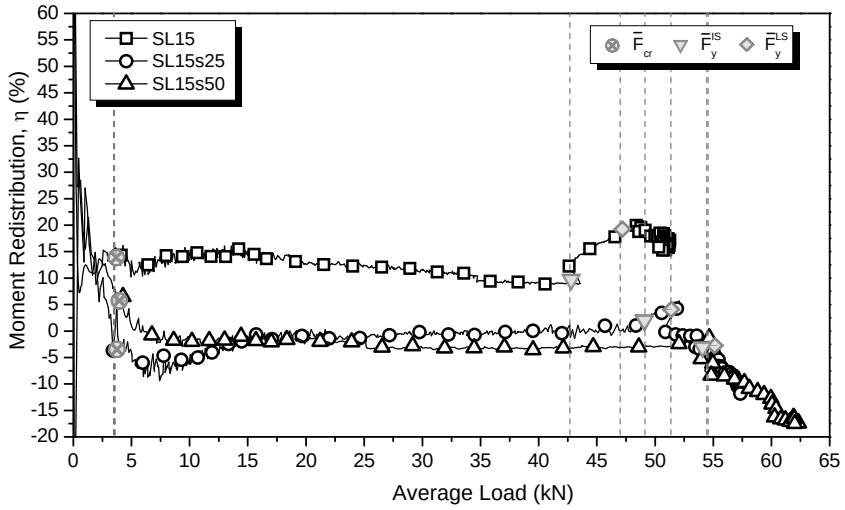

(a)

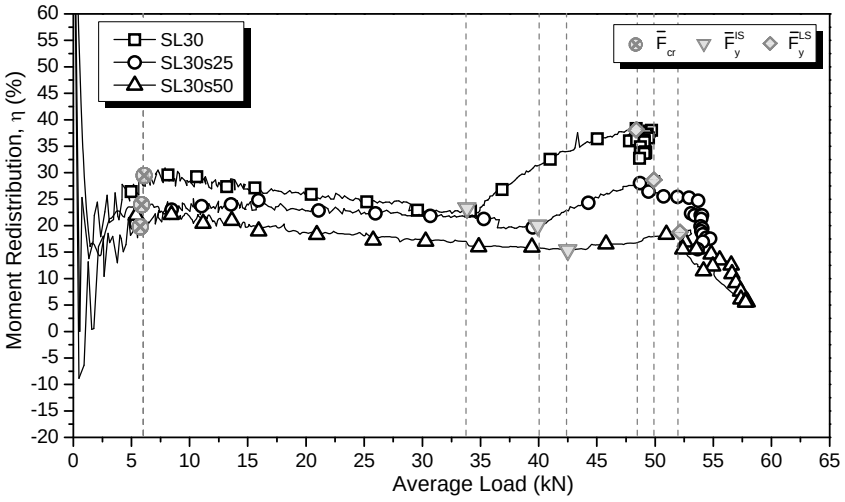

(b)

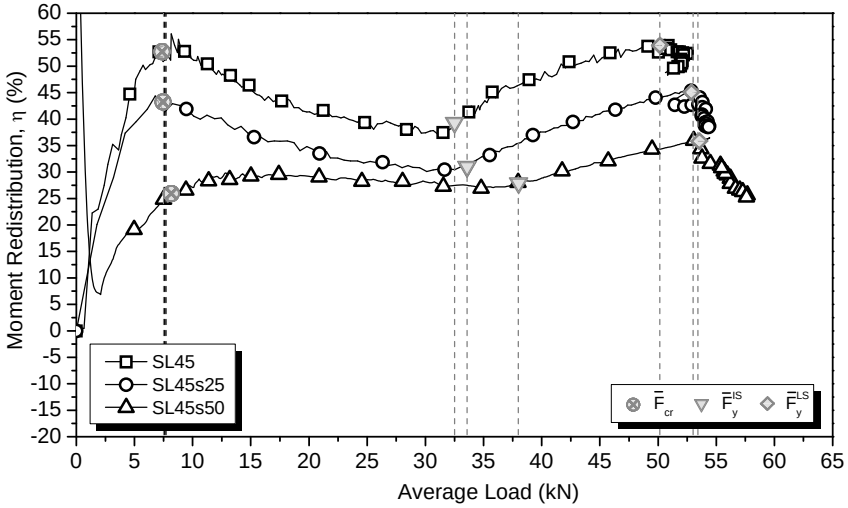

(c)

Figure 7 - Degree of moment redistribution, η, for the slab strips series: (a) SL15, (b) SL30, (c) SL45.

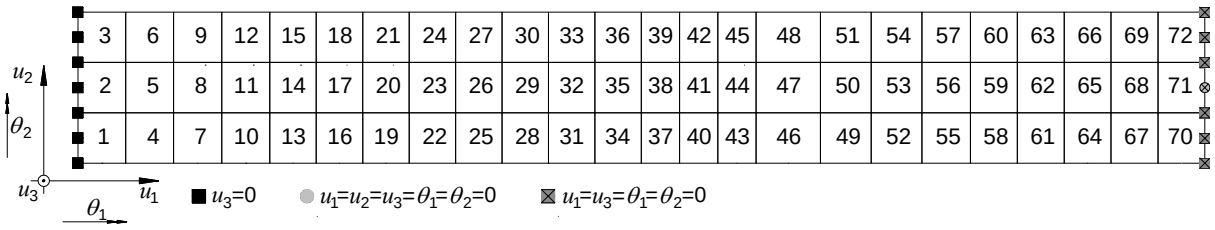

Figure 8 – Finite element mesh adopted to discretize the half part of a RC slab.

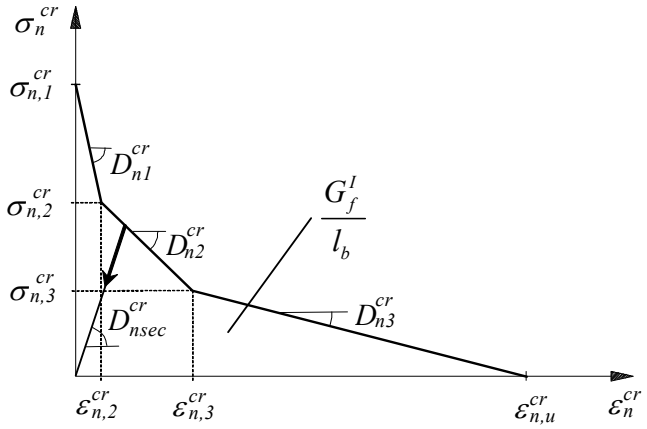

Figure 9 - Crack normal stress *vs* crack normal strain diagram for modelling the concrete tensile-softening behaviour.

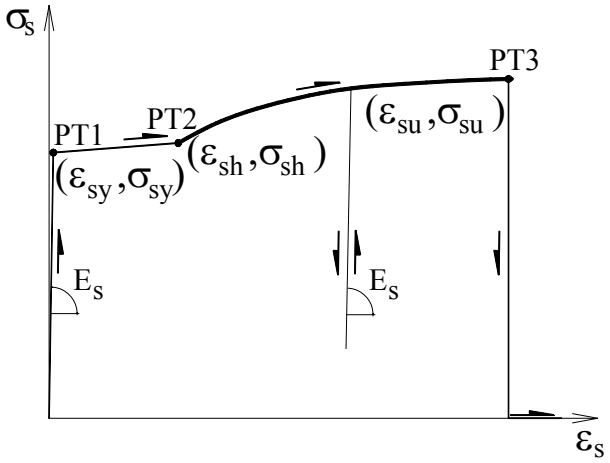

Figure 10. Uniaxial constitutive model of the rebars.

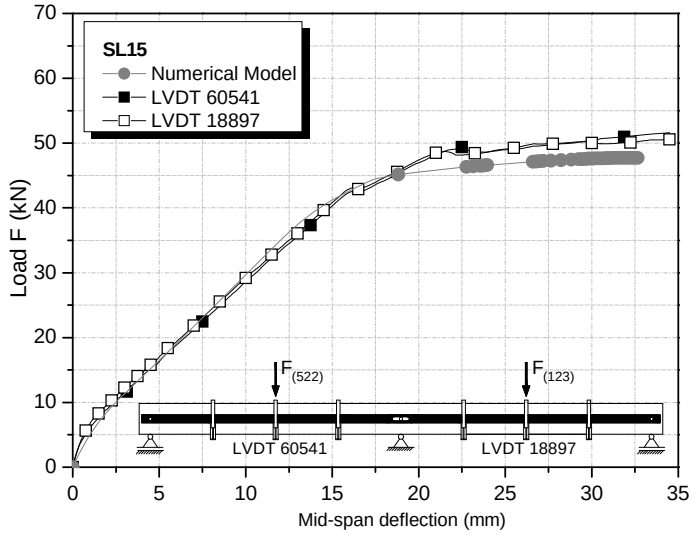

(a)

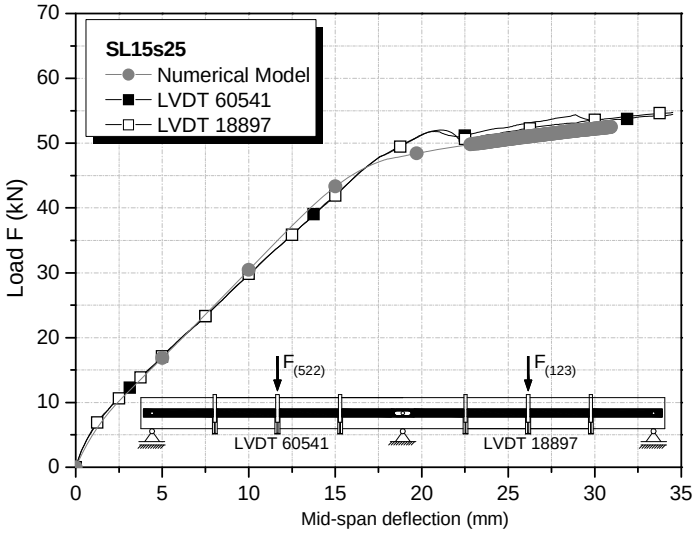

(b)

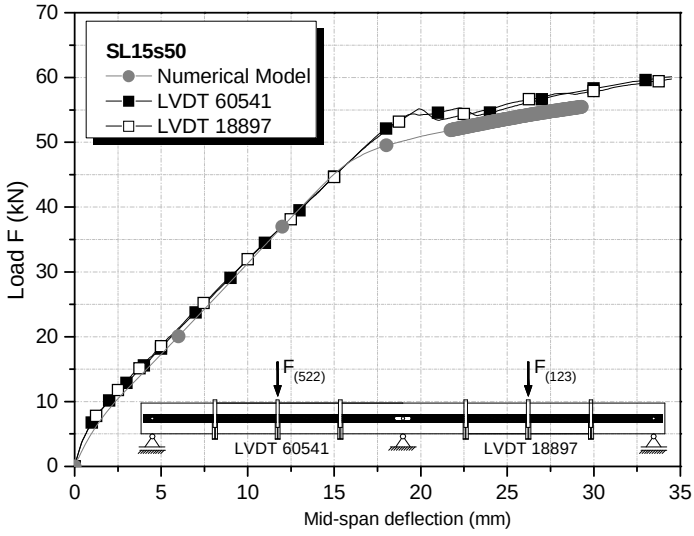

(c)

Figure 11 - Force-deflection relationship for the slabs: (a) SL15, (b) SL15s25, (c) SL15s50.

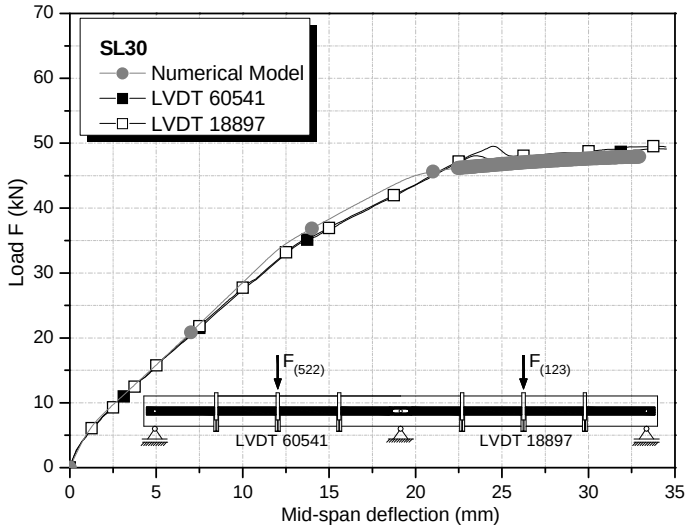

(a)

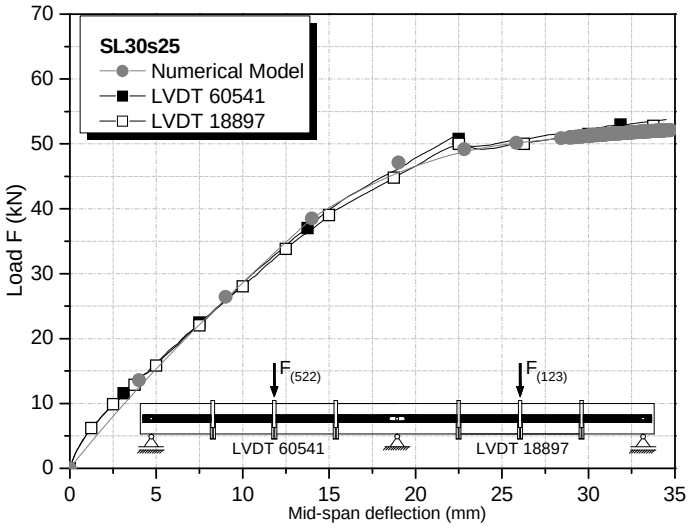

(b)

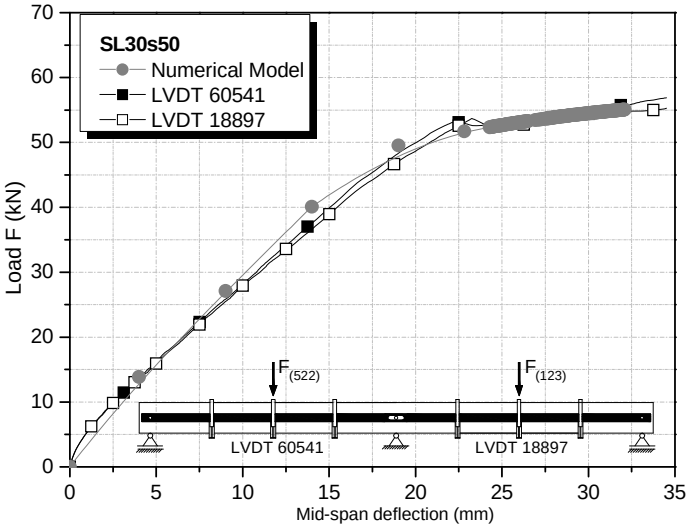

(c)

Figure 12 - Force-deflection relationship for the slabs: (a) SL30, (b) SL30s25, (c) SL30s50.

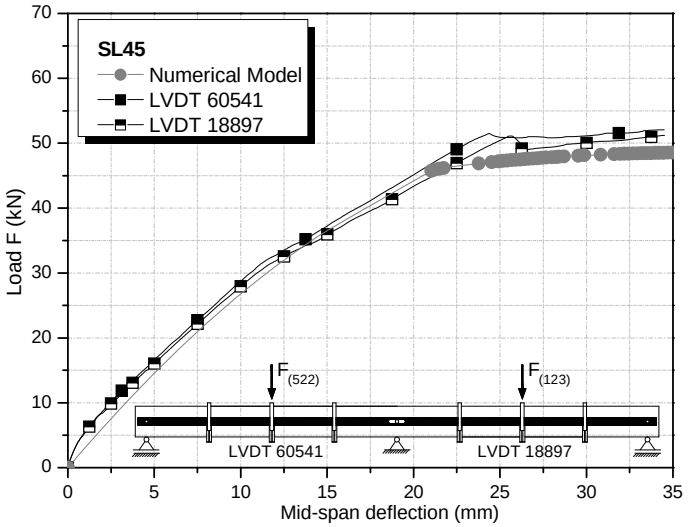

(a)

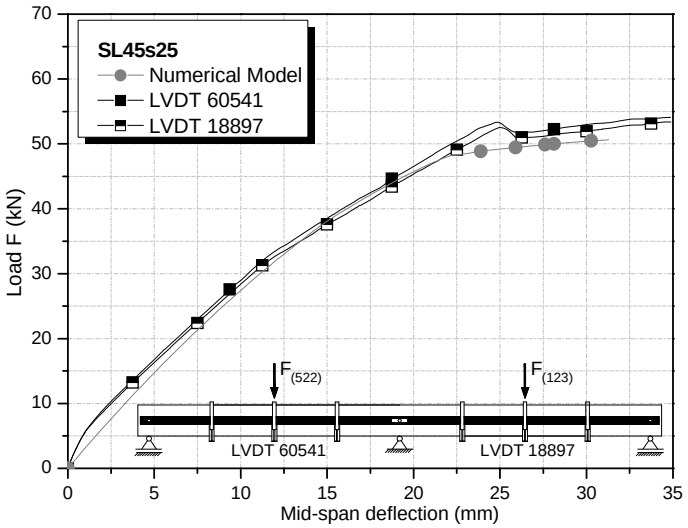

(b)

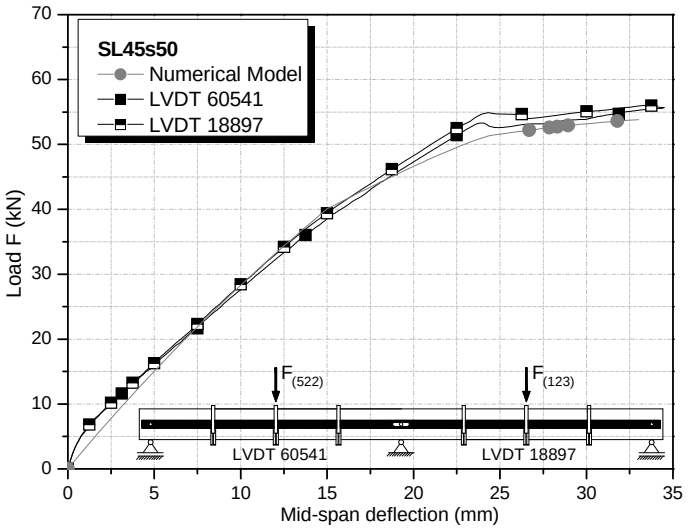

(c)

Figure 13 - Force-deflection relationship for the slabs: (a) SL45, (b) SL45s25, (c) SL45s50.

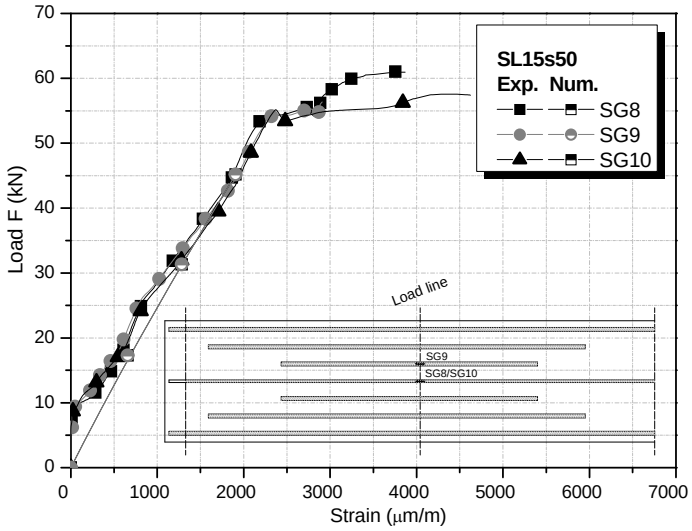

(a)

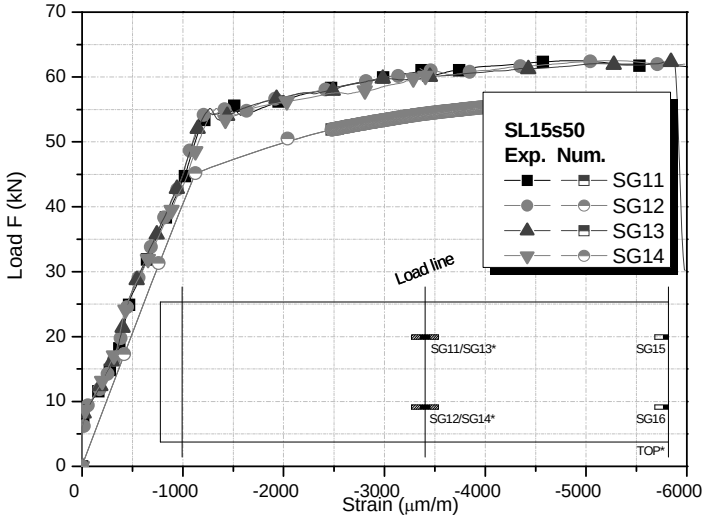

(b)

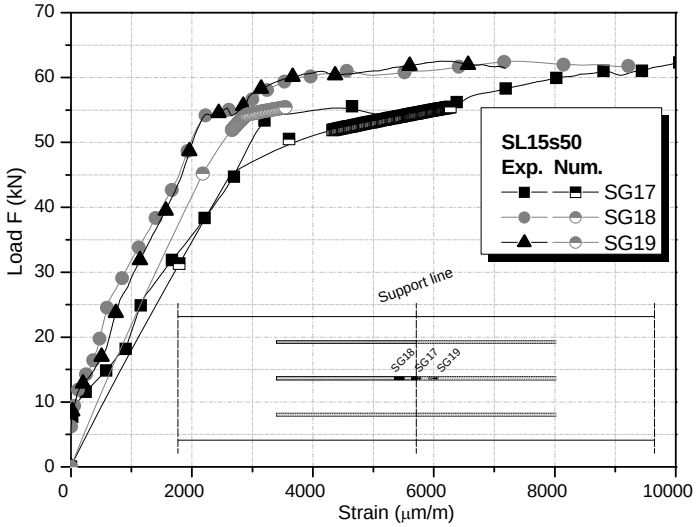

(c)

Figure 14 – SL15s50: (a) load – steel strain at slab loaded sections, (b) load – concrete strain at loaded sections, (c) load – CFRP laminate strain.

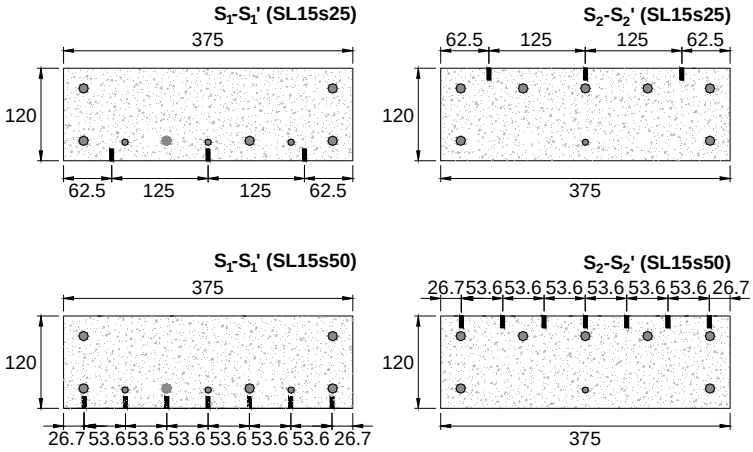

(a)

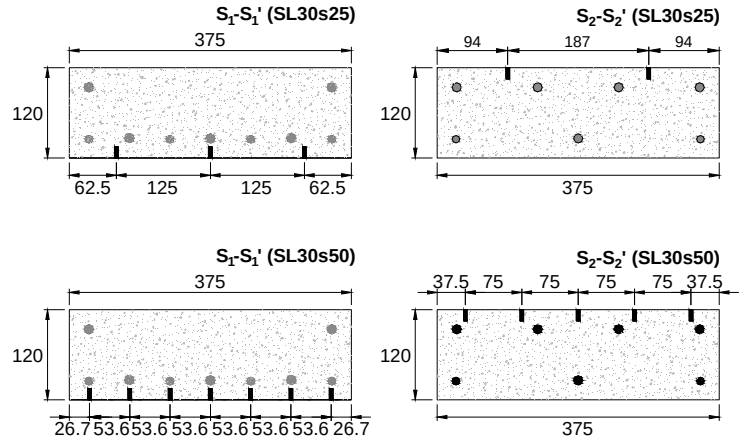

(b)

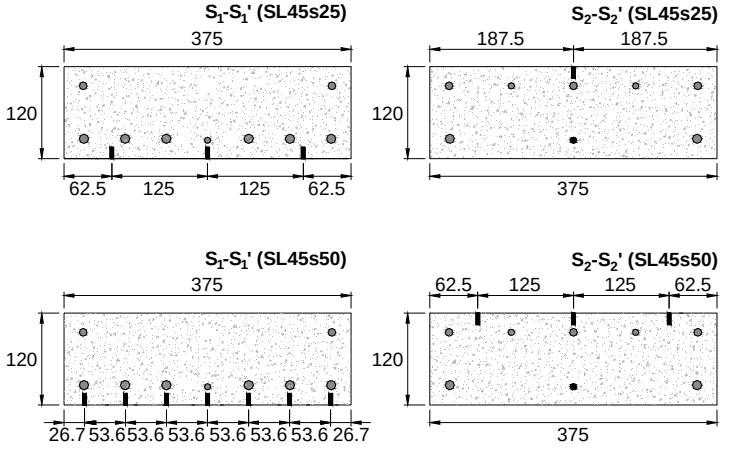

(c)

Figure 15 – Cross section dimensions and arrangements of the NSM CFRP strips for the slabs series: (a) SL15, (b) SL30 and (c) SL45.

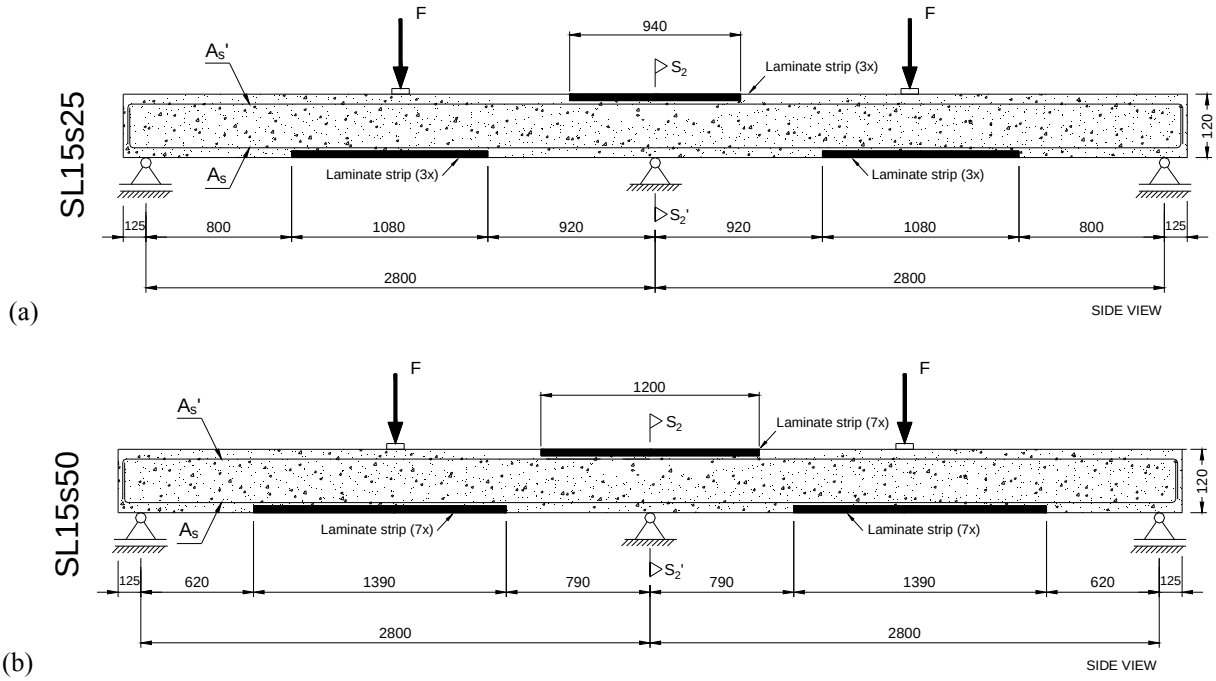

Figure 16 – CFRP strips of the two strengthened slabs of the SL15 series (dimensions in mm).

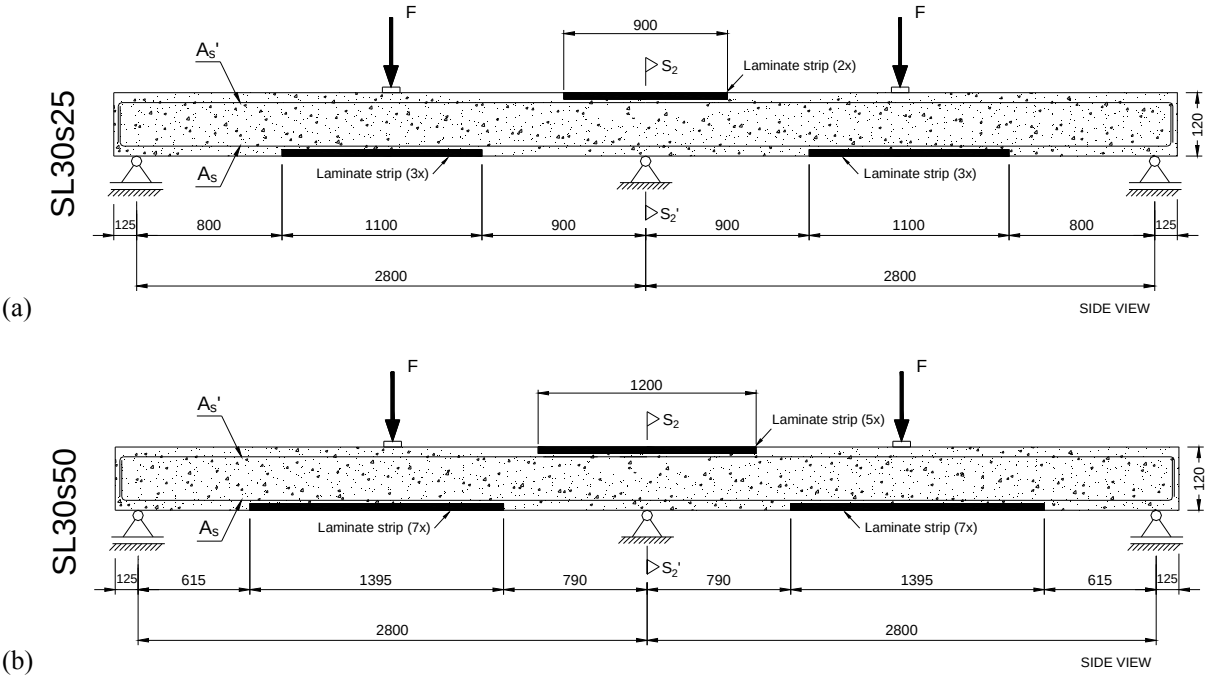

Figure 17 – CFRP strips of the two strengthened slabs of the SL30 series (dimensions in mm).

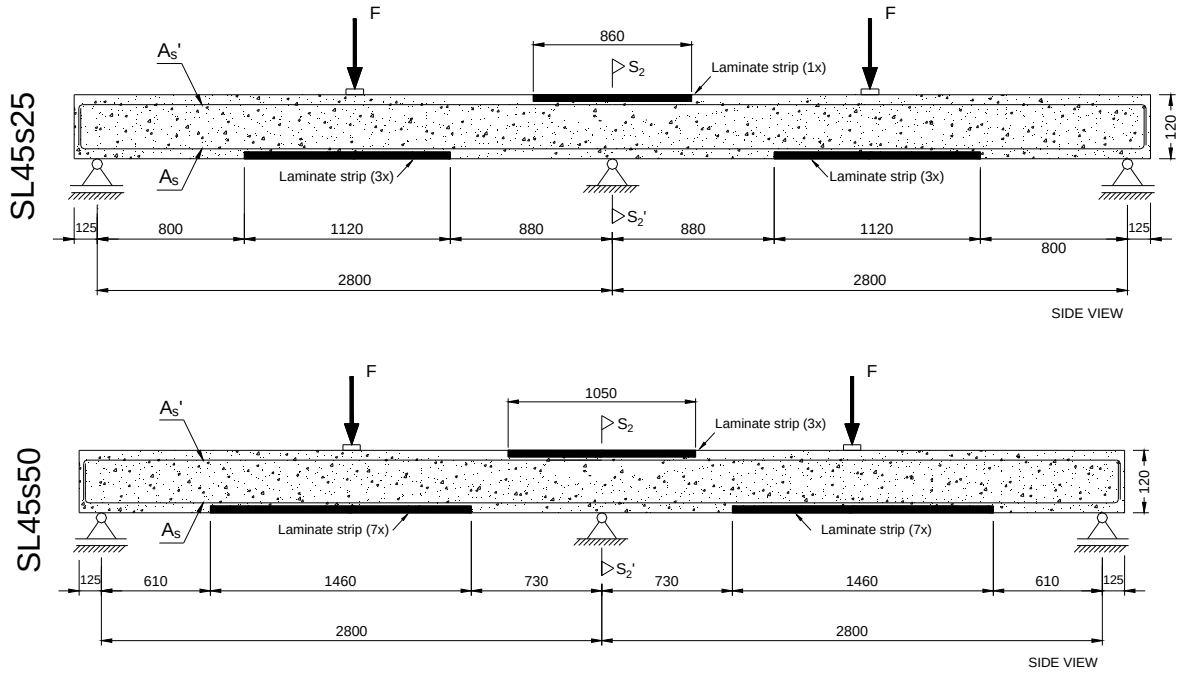

(a)

(b)

Figure 18 – CFRP strips of the two strengthened slabs of the SL45 series (dimensions in mm).

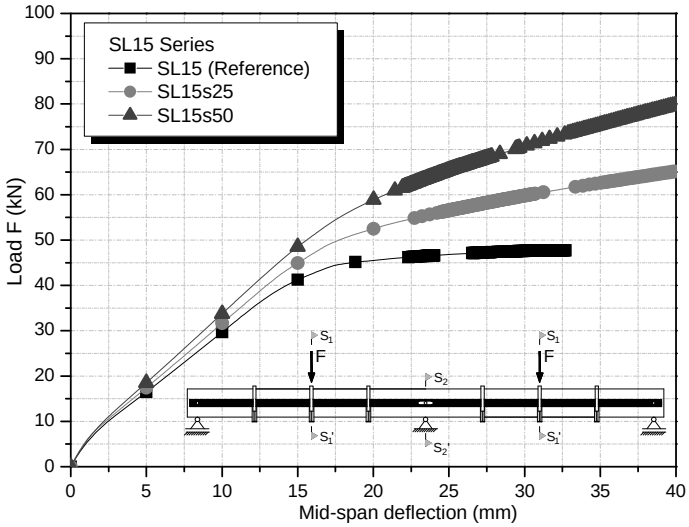

(a)

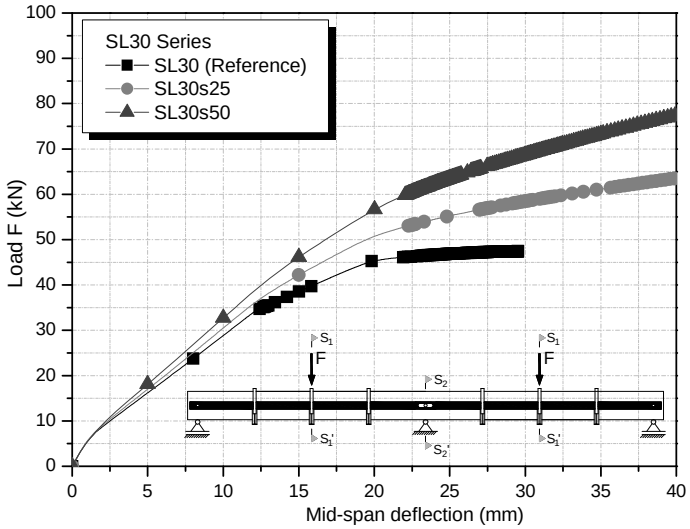

(b)

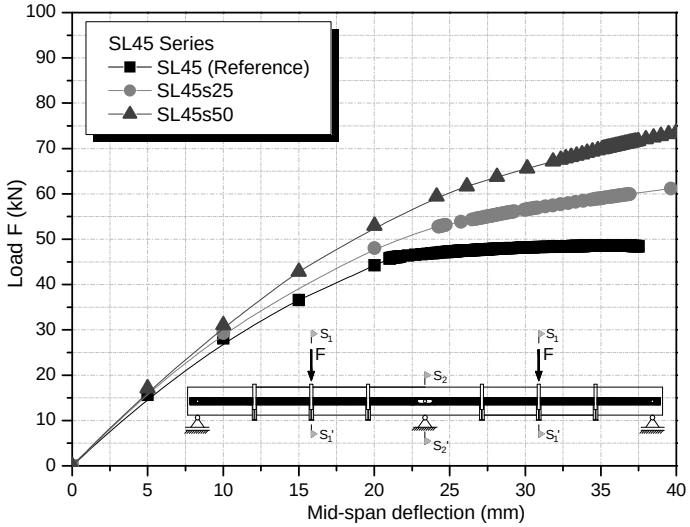

(c)

Figure 19 – Load-deflection at the loaded section for the slabs strengthened in the hogging and sagging regions: (a) SL15, (b) SL30, and (c) SL45.

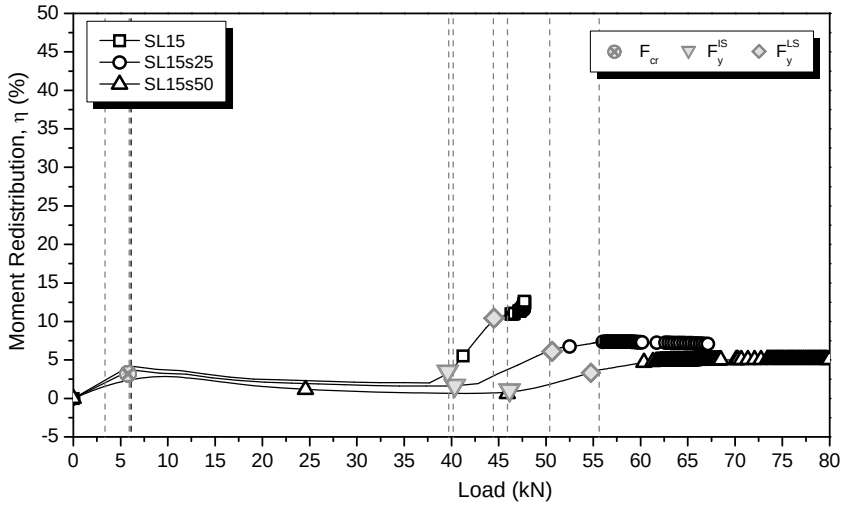

(a)

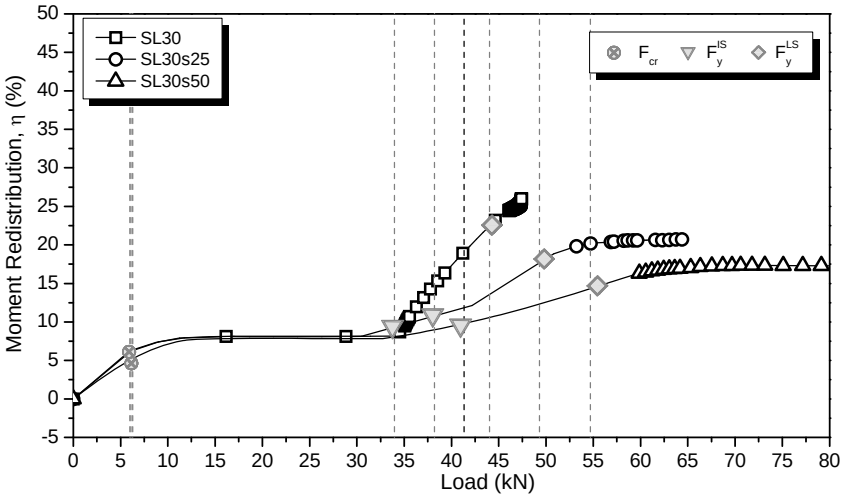

(b)

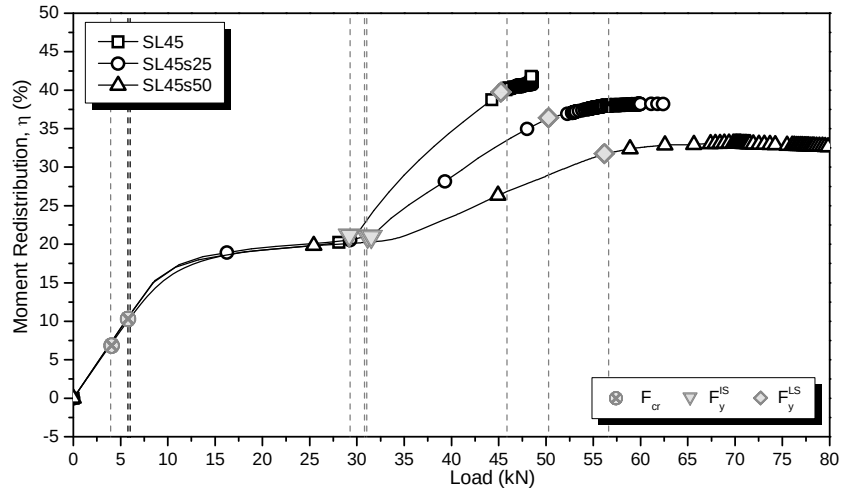

(c)

Figure 20 - Degree of moment redistribution, η, for the slab strips series strengthened in the hogging and sagging regions: (a) SL15, (b) SL30, (c) SL45.